$\bar{B} \to D^* \ell \bar{\nu}$ form factor at zero recoil from three-flavor lattice QCD: A model independent determination of $|V_{cb}|$

C. Bernard,[1] C. DeTar,[2] M. Di Pierro,[3] A. X. El-Khadra,[4] R. T. Evans,[4] E. D. Freeland,[5] E. Gamiz,[4] Steven Gottlieb,[6] U. M. Heller,[7] J. E. Hetrick,[8] A. S. Kronfeld,[9] J. Laiho,[1,9] L. Levkova,[2] P. B. Mackenzie,[9] M. Okamoto,[9] J. Simone,[9] R. Sugar,[10] D. Toussaint,[11] and R. S. Van de Water[9]

(Fermilab Lattice and MILC Collaborations)

[1]*Department of Physics, Washington University, St. Louis, Missouri, USA*
[2]*Physics Department, University of Utah, Salt Lake City, Utah, USA*
[3]*School of Computer Science, Telecommunications and Information Systems, DePaul University, Chicago, Illinois, USA*
[4]*Physics Department, University of Illinois, Urbana, Illinois, USA*
[5]*Liberal Arts Department, The School of the Art Institute of Chicago, Chicago, Illinois, USA*
[6]*Department of Physics, Indiana University, Bloomington, Indiana, USA*
[7]*American Physical Society, Ridge, New York, USA*
[8]*Physics Department, University of the Pacific, Stockton, California, USA*
[9]*Fermi National Accelerator Laboratory, Batavia, Illinois, USA*
[10]*Department of Physics, University of California, Santa Barbara, California, USA*
[11]*Department of Physics, University of Arizona, Tucson, Arizona, USA*
(Received 28 August 2008; published 22 January 2009)

We present the first lattice QCD calculation of the form factor for $\bar{B} \to D^* \ell \bar{\nu}$ with three flavors of sea quarks. We use an improved staggered action for the light valence and sea quarks (the MILC configurations), and the Fermilab action for the heavy quarks. The form factor is computed at zero recoil using a new double ratio method that yields the form factor more directly than the previous Fermilab method. Other improvements over the previous calculation include the use of much lighter light-quark masses, and the use of lattice (staggered) chiral perturbation theory in order to control the light-quark discretization errors and chiral extrapolation. We obtain for the form factor, $\mathcal{F}_{B \to D^*}(1) = 0.921(13)(20)$, where the first error is statistical and the second is the sum of all systematic errors in quadrature. Applying a 0.7% electromagnetic correction and taking the latest PDG average for $\mathcal{F}_{B \to D^*}(1)|V_{cb}|$ leads to $|V_{cb}| = (38.7 \pm 0.9_{\text{exp}} \pm 1.0_{\text{theo}}) \times 10^{-3}$.

I. INTRODUCTION

The Cabibbo-Kobayashi-Maskawa matrix element V_{cb} plays an important role in the study of flavor physics [1]. Since $|V_{cb}|$ is one of the fundamental parameters of the standard model, its value must be known precisely in order to search for new physics by looking for inconsistencies between standard model predictions and experimental measurements. For example, the standard model contribution to the kaon mixing parameter ϵ_K depends sensitively on $|V_{cb}|$ (as the fourth power), and the present errors on this quantity contribute errors to the theoretical prediction of ϵ_K that are around the same size as the errors due to B_K, the kaon bag parameter, which has been the focus of much recent work [2–5]. It is possible to obtain $|V_{cb}|$ from both inclusive and exclusive semileptonic B decays, and both determinations are limited by theoretical uncertainties. The inclusive method [6–10] makes use of the heavy-quark expansion and perturbation theory. The method also requires nonperturbative input from experiment, which is obtained from the measured moments of the inclusive

form factor $\bar{B} \to X_c \ell \bar{\nu}_\ell$ as a function of the minimum electron momentum. The dominant uncertainties in this method are the truncation of the heavy-quark expansion and perturbation theory [11,12]. In order to be competitive with the inclusive determination of $|V_{cb}|$ and thus serve as a cross-check, the exclusive method requires a reduction in the uncertainty of the $B \to D^*$ semileptonic form factor $\mathcal{F}_{B \to D^*}$, which has been calculated previously using lattice QCD in the quenched approximation [13].

Given the phenomenological importance of $|V_{cb}|$, we have revisited the calculation of $\mathcal{F}_{B \to D^*}$ at zero recoil using the $2 + 1$ flavor MILC ensembles with improved light staggered quarks [14,15]. The systematic error due to quenching is thus eliminated. The systematic error associated with the chiral extrapolation to physical light-quark masses is also reduced significantly. Since staggered quarks are computationally less expensive than many other formulations, we are able to simulate at quite small quark masses; our lightest corresponds to a pion mass of roughly 240 MeV. Given the previous experience of the MILC Collaboration with chiral fits to light meson masses and

decay constants [16], we are in a regime where we expect rooted staggered chiral perturbation theory (rSχPT) [17–21] to apply. We therefore use the rSχPT result for the $B \rightarrow D^*$ form factor [22] to perform the chiral extrapolation and to remove discretization effects particular to staggered quarks. In addition, we introduce a set of ratios that allows us to disentangle light- and heavy-quark discretization effects, and we suggest a strategy for future improvement. Finally, we extract the $B \rightarrow D^*$ form factor using a different method from that originally proposed in Ref. [13]. This new method requires many fewer three-point correlation functions, and has allowed for a savings of roughly a factor of 10 in computing resources, while at the same time simplifying the analysis.

The differential rate for the semileptonic decay $\bar{B} \rightarrow D^* \ell \bar{\nu}_\ell$ is

$$\frac{d\Gamma}{dw} = \frac{G_F^2}{4\pi^3} m_{D^*}^3 (m_B - m_{D^*})^2 \sqrt{w^2 - 1}$$
$$\times \mathcal{G}(w) |V_{cb}|^2 |\mathcal{F}_{B \rightarrow D^*}(w)|^2, \quad (1)$$

where $w = v' \cdot v$ is the velocity transfer from the initial state to the final state, and $\mathcal{G}(w) |\mathcal{F}_{B \rightarrow D^*}(w)|^2$ contains a combination of four form factors that must be calculated nonperturbatively. At zero recoil $\mathcal{G}(1) = 1$, and $\mathcal{F}_{B \rightarrow D^*}(1)$ reduces to a single form factor $h_{A_1}(1)$. Given $h_{A_1}(1)$, the measured decay rate determines $|V_{cb}|$.

The quantity h_{A_1} is a form factor of the axial-vector current

$$\langle D^*(v, \epsilon') | \mathcal{A}^\mu | \bar{B}(v) \rangle = i\sqrt{2m_B 2m_{D^*}} \bar{\epsilon}'^\mu h_{A_1}(1), \quad (2)$$

where $\mathcal{A}^\mu$ is the continuum axial-vector current and ϵ' is the polarization vector of the D^*. Heavy-quark symmetry plays a useful role in constraining $h_{A_1}(1)$, leading to the heavy-quark expansion [23,24]

$$h_{A_1}(1) = \eta_A \left[1 - \frac{\ell_V}{(2m_c)^2} + \frac{2\ell_A}{2m_c 2m_b} - \frac{\ell_P}{(2m_b)^2} \right], \quad (3)$$

up to order $1/m_Q^2$, and where η_A is a factor that matches heavy-quark effective theory (HQET) to QCD [25,26]. The ℓ's are long-distance matrix elements of the HQET. Heavy-quark symmetry forbids terms of order $1/m_Q$ at zero recoil [27], and various methods have been used to compute the size of the $1/m_Q^2$ coefficients, including quenched lattice QCD [13].

The earlier work by Hashimoto *et al.* [13] used three double ratios in order to obtain separately each of the three $1/m_Q^2$ coefficients in Eq. (3). These three double ratios also determine three out of the four coefficients appearing at $1/m_Q^3$ in the heavy-quark expansion. It was shown in Ref. [28] that, for the Fermilab method matched to tree level in α_s and to next-to-leading order in HQET, the leading discretization errors for the double ratios for this quantity are of order $\alpha_s(\bar{\Lambda}/2m_Q)^2 f_{\mathcal{B}}(am_Q)$ and

$(\bar{\Lambda}/2m_Q)^3 f_i(am_Q)$, where $\bar{\Lambda}$ is a QCD scale stemming from the light degrees of freedom, such as that appearing in the HQET expansion for the heavy-light meson mass $m_M = m_Q + \bar{\Lambda} + \cdots$. The functions $f_i(am_Q)$ are coefficients depending on am_Q and α_s, but not on $\bar{\Lambda}$. When $am_Q \sim 1$, the $f_i(am_Q)$ are of order one; when $am_Q \ll 1$, they go like a power of am_Q, such that the continuum limit is obtained. The powers of 2 are combinatoric factors.

As discussed in Ref. [13], all uncertainties in the double ratios $\mathcal{R}$ used in that work scale as $\mathcal{R} - 1$ rather than as $\mathcal{R}$. Statistical errors in the numerator and denominator are highly correlated and largely cancel in these double ratios. Also, most of the normalization uncertainty in the lattice currents cancels, leaving a normalization factor close to 1, which can be computed reliably in perturbation theory. Finally, the quenching error, relevant to Ref. [13] but not to the present unquenched calculation, scales as $\mathcal{R} - 1$ rather than as $\mathcal{R}$. This scaling of the error occurs because the double ratios constructed in Ref. [13] become the identity in the limit of equal bottom and charm quark masses.

In the calculation reported here, the form factor $h_{A_1}(1)$ is computed more directly using only one double ratio

$$\mathcal{R}_{A_1} = \frac{\langle D^* | \bar{c}\gamma_j \gamma_5 b | \bar{B} \rangle \langle \bar{B} | \bar{b}\gamma_j \gamma_5 c | D^* \rangle}{\langle D^* | \bar{c}\gamma_4 c | D^* \rangle \langle \bar{B} | \bar{b}\gamma_4 b | \bar{B} \rangle} = |h_{A_1}(1)|^2, \quad (4)$$

which is exact to all orders in the heavy-quark expansion in the continuum.[1] The lattice approximation to this ratio still has discretization errors that are suppressed by inverse powers of heavy-quark masses [$\alpha_s(\bar{\Lambda}/2m_Q)^2$ and $(\bar{\Lambda}/2m_Q)^3$], but which again vanish in the continuum limit. The errors in the ratio introduced in Eq. (4) do not scale rigorously as $\mathcal{R}_{A_1} - 1$ because $\mathcal{R}_{A_1}$ is not one in the limit of equal bottom and charm quark masses. Nevertheless, this double ratio still retains the desirable features of the previous double ratios, i.e., large statistical error cancellations and the cancellation of most of the lattice current renormalization. Because the quenching error has been eliminated, the rigorous scaling of all the errors as $\mathcal{R} - 1$, including the quenching error, is no longer crucial. The more direct method introduced here has the significant advantage that extracting coefficients from fits to HQET expressions as a function of heavy-quark masses is not necessary, and no error is introduced from truncating the heavy-quark expansion to a fixed order in $1/m_Q^n$. In short, for an unquenched QCD calculation, the method using Eq. (4) gives a smaller total error than the method used in Ref. [13] for a fixed amount of computer time.

The currents of lattice gauge theory must be matched to the normalization of the continuum to obtain $\mathcal{R}_{A_1}$. The matching factors mostly cancel in the double ratio [29,30],

---

[1]Note that the notation $\mathcal{R}_{A_1}$ stands for a different double ratio in Ref. [13].

leaving $h_{A_1}(1) = \sqrt{\mathcal{R}_{A_1}} = \rho \sqrt{R_{A_1}}$, where R_{A_1} is the lattice double ratio and ρ, the ratio of matching factors, is very close to 1. (For the remainder of this paper we shall use the convention that a script letter corresponds to a continuum quantity, while a nonscript letter corresponds to a lattice quantity.) This ρ factor has been calculated to one-loop order in perturbative QCD, and is found to contribute less than a 0.5% correction. We have exploited the ρ factors to implement a blind analysis. Two of us involved in the perturbative calculation applied a common multiplicative offset to the ρ factors needed to obtain $h_{A_1}(1)$ at different lattice spacings. This offset was not disclosed to the rest of us until the procedure for determining the systematic error budget for the rest of the analysis had been finalized.

The unquenched MILC configurations generated with $2 + 1$ flavors of improved staggered fermions make use of the fourth-root procedure for eliminating the unwanted four-fold degeneracy of staggered quarks. At nonzero lattice spacing, this procedure has small violations of unitarity [31–35] and locality [36]. Nevertheless, a careful treatment of the continuum limit, in which all assumptions are made explicit, argues that lattice QCD with rooted staggered quarks reproduces the desired local theory of QCD as $a \to 0$ [37,38]. When coupled with other analytical and numerical evidence (see Refs. [39–41] for reviews), this gives us confidence that the rooting procedure is indeed correct in the continuum limit.

The outline of the rest of this paper is as follows: Section II describes the details of the lattice simulation. Section III discusses the fits to the double ratios accounting for oscillating opposite-parity states. Section IV summarizes the lattice perturbation theory calculation of the ρ factor. Section V introduces the rooted staggered chiral perturbation theory formalism and expressions used in the chiral extrapolations. Section VI then discusses our treatment of the chiral extrapolation and introduces our approach for disentangling heavy- and light-quark discre-

tization effects. Section VII provides a detailed discussion of our systematic errors, and we conclude in Sec. VIII.

II. LATTICE CALCULATION

The lattice calculation was done on the MILC ensembles at three lattice spacings with $a \approx 0.15$, 0.125, and 0.09 fm; these ensembles have an $O(a^2)$ Symanzik improved gauge action and $2 + 1$ flavors of "AsqTad" improved staggered sea quarks [42–47]. The parameters for the MILC lattices used in this calculation are shown in Table I. We have several light masses at both full QCD and partially quenched points ($m_{\text{val}} \neq m_{\text{sea}}$), and our light-quark masses range between $m_s/10$ and $m_s/2$. Table II shows the valence masses computed on each ensemble. In this work we follow the notation [16], where m_s is the physical strange quark mass, $\hat{m}$ is the average u-d quark mass, and $\hat{m}'$, m_s' indicate the nominal values used in simulations. In practice, the MILC ensembles choose m_s' within 10–30% of m_s and a range of $\hat{m}'$ to enable a chiral extrapolation.

The heavy quarks are computed using the Sheikholeslami-Wohlert (SW) "clover" action [48] with the Fermilab interpretation via HQET [49]. The SW action includes a dimension-five interaction with a coupling c_{SW} that has been adjusted to the value u_0^{-3} suggested by tadpole-improved, tree-level perturbation theory [50]. The value of u_0 is calculated either from the plaquette ($a \approx 0.15$ fm and $a \approx 0.09$ fm), or from the Landau link ($a \approx 0.12$ fm). The adjustment of c_{SW} is needed to normalize the heavy quark's chromomagnetic moment correctly [49].

The tadpole-improved bare quark mass for SW quarks is given by

$$am_0 = \frac{1}{u_0}\left(\frac{1}{2\kappa} - \frac{1}{2\kappa_{\text{crit}}}\right), \tag{5}$$

where tuning the parameter κ to the critical quark hopping parameter κ_{crit} would lead to a massless pion. The spin-averaged B_s and D_s kinetic masses are computed on a

TABLE I. Parameters of the simulations. The columns from left to right are the approximate lattice spacing in fm, the sea quark masses $a\hat{m}'/am_s'$, the linear spatial dimension of the lattice ensemble in fm, the dimensionless factor $m_\pi L$ (m_π corresponds to the taste-pseudoscalar pion composed of light sea quarks), the gauge coupling, the dimensions of the lattice in lattice units, the number of configurations used for this analysis, the bare hopping parameter used for the bottom quark, the bare hopping parameter used for the charm quark, and the clover term c_{SW} used for both bottom and charm quarks.

a (fm)	$a\hat{m}'/am_s'$	L (fm)	$m_\pi L$	$10/g^2$	Volume	# Configs	κ_b	κ_c	c_{SW}
0.15	0.0194/0.0484	2.4	5.5	6.586	$16^3 \times 48$	628	0.076	0.122	1.5673
0.15	0.0097/0.0484	2.4	3.9	6.572	$16^3 \times 48$	628	0.076	0.122	1.5673
0.12	0.02/0.05	2.4	6.2	6.79	$20^3 \times 64$	460	0.086	0.122	1.72
0.12	0.01/0.05	2.4	4.5	6.76	$20^3 \times 64$	592	0.086	0.122	1.72
0.12	0.007/0.05	2.4	3.8	6.76	$20^3 \times 64$	836	0.086	0.122	1.72
0.12	0.005/0.05	2.9	3.8	6.76	$24^3 \times 64$	528	0.086	0.122	1.72
0.09	0.0124/0.031	2.4	5.8	7.11	$28^3 \times 96$	516	0.0923	0.127	1.476
0.09	0.0062/0.031	2.4	4.1	7.09	$28^3 \times 96$	556	0.0923	0.127	1.476
0.09	0.0031/0.031	3.4	4.2	7.08	$40^3 \times 96$	504	0.0923	0.127	1.476

TABLE II. Valence masses used in the simulations. The columns from left to right are the approximate lattice spacing in fm, the sea quark masses $a\hat{m}'/am'_s$ identifying the gauge ensemble, and the valence masses computed on that ensemble.

a (fm)	$a\hat{m}'/am'_s$	am_x
≈ 0.15	0.0194/0.0484	0.0194
≈ 0.15	0.0097/0.0484	0.0097, 0.0194
≈ 0.12	0.02/0.05	0.02
≈ 0.12	0.01/0.05	0.01, 0.02
≈ 0.12	0.007/0.05	0.007, 0.02
≈ 0.12	0.005/0.05	0.005, 0.02
≈ 0.09	0.0124/0.031	0.0124
≈ 0.09	0.0062/0.031	0.0062, 0.0124
≈ 0.09	0.0031/0.031	0.0031, 0.0124

subset of the ensembles in order to tune the bare κ values for bottom and charm (and hence the corresponding bare quark masses) to their physical values. These tuned values were then used in the $B \to D^*\ell\nu$ form-factor production run.

The relative lattice scale is determined by calculating r_1/a on each ensemble, where r_1 is related to the force between static quarks by $r_1^2 F(r_1) = 1.0$ [51,52]. To avoid introducing implicit dependence on $\hat{m}'$, m'_s via $r_1(\hat{m}', m'_s, g^2)$ (where, as above, primes denote simulation masses), we interpolate in m'_s and extrapolate in $\hat{m}'$ to obtain $r_1(\hat{m}, m_s, g^2)/a$ at the physical masses. We then convert from lattice units to r_1 units with $r_1(\hat{m}, m_s, g^2)/a$. Below we shall call this procedure the mass-independent determination of r_1.

In order to fix the absolute lattice scale, one must compute a physical quantity that can be compared directly to experiment; we use the Υ 2S-1S splitting [53] and the most recent MILC determination of f_π [54]. The difference between these determinations results in a systematic error that turns out to be much smaller than our other systematics. When the Υ scale determination is combined with the continuum extrapolated r_1 value at physical quark masses, a value $r_1^{\mathrm{phys}} = 0.318(7)$ fm [55] is obtained. The f_π determination is $r_1^{\mathrm{phys}} = 0.3108(15)(^{+26}_{-79})$ fm [54]. Given r_1^{phys}, it is then straightforward to convert quantities measured in r_1 units to physical units.

The dependence on the lattice spacing a is mild in this analysis. Since a only enters the calculation through the adjustment of the heavy- and light-quark masses, the dependence of $h_{A_1}(1)$ on a is small. Staggered chiral perturbation theory indicates that the a dependence coming from staggered-quark discretization effects is small [22], and this is consistent with the simulation data.

In this work, we construct lattice currents as in Ref. [49],

$$J_\mu^{hh'} = \sqrt{Z_{V_4}^{hh} Z_{V_4}^{h'h'}}\, \bar{\Psi}_h \Gamma_\mu \Psi_{h'}, \qquad (6)$$

where Γ_μ is either the vector ($i\gamma^\mu$) or axial-vector ($i\gamma^\mu \gamma_5$)

current. The rotated field Ψ_h is defined by

$$\Psi_h = (1 + ad_1\boldsymbol{\gamma} \cdot \mathbf{D}_{\mathrm{lat}})\psi_h, \qquad (7)$$

where ψ_h is the (heavy) lattice quark field in the SW action. $\mathbf{D}_{\mathrm{lat}}$ is the symmetric, nearest-neighbor, covariant difference operator; the tree-level improvement coefficient is

$$d_1 = \frac{1}{u_0}\left(\frac{1}{2 + m_0 a} - \frac{1}{2(1 + m_0 a)}\right). \qquad (8)$$

In Eq. (6) we choose to normalize the current by the factors of $Z_{V_4}^{hh}$ ($h = c, b$) since even for massive quarks they are easy to compute nonperturbatively. The continuum current is related to the lattice current by

$$\mathcal{J}_\mu^{hh'} = \rho_{J_\Gamma} J_\mu^{hh'} \qquad (9)$$

up to discretization effects, where

$$\rho_{J_\Gamma}^2 = \frac{Z_{J_\Gamma}^{bc} Z_{J_\Gamma}^{cb}}{Z_{V_4}^{cc} Z_{V_4}^{bb}}, \qquad (10)$$

and the matching factors $Z_{J_\Gamma}^{hh'}$'s are defined in Ref. [30]. Note that the factor $\sqrt{Z_{V_4}^{bb} Z_{V_4}^{cc}}$ multiplying the lattice current in Eq. (6) cancels in the double ratio by design, leaving only the ρ factor, which is close to 1 and can be computed reliably using perturbation theory. The perturbative calculation of ρ_{J_Γ} is described in more detail in Sec. IV.

Interpolating operators are constructed from four-component heavy quarks and staggered quarks as follows: Let

$$\mathcal{O}_{D_j^*}(x) = \bar{\chi}(x)\Omega^\dagger(x)i\gamma_j\psi_c(x), \qquad (11)$$

$$\mathcal{O}_B^\dagger(x) = \bar{\psi}_b(x)\gamma_5\Omega(x)\chi(x), \qquad (12)$$

where χ is the one-component field in the staggered-quark action, and

$$\Omega(x) = \gamma_1^{x_1/a}\gamma_2^{x_2/a}\gamma_3^{x_3/a}\gamma_4^{x_4/a}. \qquad (13)$$

The left (right) index of $\Omega^\dagger$ (Ω) can be left as a free taste index [41] or χ can be promoted to a four-component naive-quark field to contract all indices [56]. The resulting correlation functions are the same if the initial and final taste indices are set equal and then summed. The same kinds of operators have been used in previous calculations [57–59].

Lattice matrix elements are obtained from three-point correlation functions. The three-point correlation functions needed for the $B \to D^*$ transition at zero-recoil are

$$C^{B \to D^*}(t_i, t_s, t_f) = \sum_{\mathbf{x},\mathbf{y}} \langle 0|\mathcal{O}_{D^*}(\mathbf{x}, t_f)\bar{\Psi}_c\gamma_j\gamma_5\Psi_b(\mathbf{y}, t_s)$$

$$\times \mathcal{O}_B^\dagger(\mathbf{0}, t_i)|0\rangle, \qquad (14)$$

$$C^{B \to B}(t_i, t_s, t_f) = \sum_{\mathbf{x, y}} \langle 0 | \mathcal{O}_B(\mathbf{x}, t_f) \bar{\Psi}_b \gamma_4 \Psi_b(\mathbf{y}, t_s)$$
$$\times \mathcal{O}_B^\dagger(\mathbf{0}, t_i) | 0 \rangle, \tag{15}$$

$$C^{D^* \to D^*}(t_i, t_s, t_f) = \sum_{\mathbf{x, y}} \langle 0 | \mathcal{O}_{D^*}(\mathbf{x}, t_f) \bar{\Psi}_c \gamma_4 \Psi_c(\mathbf{y}, t_s)$$
$$\times \mathcal{O}_{D^*}^\dagger(\mathbf{0}, t_i) | 0 \rangle. \tag{16}$$

In $C^{B \to D^*}$ the polarization of the D^* lies along spatial direction j. If the source-sink separation is large enough, then we can arrange for both $t_s - t_i$ and $t_f - t_s$ to be large so that the lowest-lying state dominates. Then

$$C^{B \to D^*}(t_i, t_s, t_f) = Z_{D^*}^{1/2} Z_B^{1/2} \frac{\langle D^* | \bar{\Psi}_c \gamma_j \gamma_5 \Psi_b | B \rangle}{\sqrt{2 m_{D^*}} \sqrt{2 m_B}}$$
$$\times e^{-m_B(t_s - t_i)} e^{-m_{D^*}(t_f - t_s)} + \dots, \tag{17}$$

where m_B and m_{D^*} are the masses of the B and D^* mesons and $Z_H = |\langle 0 | \mathcal{O}_H | H \rangle|^2$.

In practice, the meson source and sink are held at fixed $t_i = 0$ and $t_f = T$, while the operator time $t_s = t$ is varied over all times in between. Using the correlators defined in Eqs. (14)–(16) we form the double ratio

$$R_{A_1}(t) = \frac{C^{B \to D^*}(0, t, T) C^{D^* \to B}(0, t, T)}{C^{D^* \to D^*}(0, t, T) C^{B \to B}(0, t, T)}. \tag{18}$$

All convention-dependent normalization factors, including the factors of $\sqrt{Z_H / 2 m_H}$, cancel in the double ratio. In the window of time separations where the ground state dominates, a plateau should be visible, and the lattice ratio is simply related to the continuum ratio $\mathcal{R}_{A_1}$ by a renormalization factor

$$\rho_{A_1} \sqrt{R_{A_1}} = \sqrt{\mathcal{R}_{A_1}} = h_{A_1}(1), \tag{19}$$

with ρ_{A_1} as in Eq. (10). The right-hand side of Eq. (17) is the first term in a series, with additional terms for each radial excitation, including opposite-parity states that arise with staggered quarks. Eliminating the opposite-parity states requires some care, and this is discussed in detail in the next section. In order to isolate the lowest-lying states we have chosen creation and annihilation operators, $\mathcal{O}_B^\dagger$ and $\mathcal{O}_{D^*}$, which have a large overlap with the desired state. This was done by smearing the heavy quark and antiquark propagator sources with 1S Coulomb-gauge wave functions.

III. FITTING AND OPPOSITE-PARITY STATES

Extracting correlation functions of operators with staggered quarks presents an extra complication because the contributions of opposite-parity states introduce oscillations in time into the correlator fits [56]. Three-point functions obey the functional form

$$C^{X \to Y}(0, t, T) = \sum_{k=0}^{\infty} \sum_{\ell=0}^{\infty} (-1)^{kt}$$
$$\times (-1)^{\ell(T-t)} A_{\ell k} e^{-m_X^{(k)} t} e^{-m_Y^{(\ell)}(T-t)}. \tag{20}$$

For odd k and ℓ the excited-state contributions change sign as the position of the operator varies by one time slice. Although they are exponentially suppressed, the parity partners of the heavy-light mesons are not that much heavier than the ground states in which we are interested, so the oscillations can be significant at the source-sink separations typical of our calculations. These separations cannot be too large because of the rapid decrease of the signal due to the presence of the heavy quark.

Although one can fit a given three-point correlator to Eq. (20), in the calculation of $h_{A_1}(1)$ we use double ratios in which numerator and denominator are so similar that most of the fitting systematics cancel, and it is convenient to preserve this simplifying feature. We do this by forming a suitable average over correlator ratios with different (even and odd) source-sink separations. It turns out that the amplitudes of the oscillating states in $B \to D^*$ correlation functions are much smaller than they are in many other heavy-light transitions [60,61], and that the oscillating states in $B \to D^*$ are barely visible at the present level of statistics. Even so, we introduce an average that reduces them still further, to the point where they are negligible.

Although we shall take the average of the double ratio, let us first examine the average of an individual three-point function. Expanding Eq. (20) so that it includes the ground state and the first oscillating state, we have

$$C^{X \to Y}(0, t, T) = A_{00}^{X \to Y} e^{-m_X t - m_Y(T-t)}$$
$$+ (-1)^{T-t} A_{01}^{X \to Y} e^{-m_X t - m_Y'(T-t)}$$
$$+ (-1)^t A_{10}^{X \to Y} e^{-m_X' t - m_Y(T-t)}$$
$$+ (-1)^T A_{11}^{X \to Y} e^{-m_X' t - m_Y'(T-t)} + \dots$$
$$= A_{00}^{X \to Y} e^{-m_X t - m_Y(T-t)} [1 + c^{X \to Y}(0, t, T)$$
$$+ \dots], \tag{21}$$

where in the last line we have pulled out the ground state amplitude and exponential dependence. The function $c^{X \to Y}(0, t, T)$ is defined

$$c^{X \to Y}(0, t, T) \equiv \frac{A_{01}^{X \to Y}}{A_{00}^{X \to Y}} (-1)^{T-t} e^{-\Delta m_Y(T-t)}$$
$$+ \frac{A_{10}^{X \to Y}}{A_{00}^{X \to Y}} (-1)^t e^{-\Delta m_X t}$$
$$+ \frac{A_{11}^{X \to Y}}{A_{00}^{X \to Y}} (-1)^T e^{-\Delta m_X t - \Delta m_Y(T-t)}, \tag{22}$$

where $\Delta m_{X, Y} = m_{X, Y}' - m_{X, Y}$ is the splitting between the lowest-lying desired-parity state and the lowest-lying wrong-parity state. Note that the first two terms produce oscillations as the position of the operator is varied over the

time extent of the lattice. The third term, however, changes sign only when the total source-sink separation is varied. It is this term that our average is designed to suppress, since it will not be as clearly visible in the t dependence of the lattice data as those that oscillate in t.

We define the average to be

$$\bar{C}^{X\to Y}(0, t, T) \equiv \tfrac{1}{2}C^{X\to Y}(0, t, T) + \tfrac{1}{4}C^{X\to Y}(0, t, T + 1)$$
$$+ \tfrac{1}{4}C^{X\to Y}(0, t + 1, T + 1). \quad (23)$$

Substituting the expression for $C^{X\to Y}(0, t, T)$ from Eq. (21) into this definition gives

$$\bar{C}^{X\to Y}(0, t, T) = A_{00}^{X\to Y}e^{-m_X t - m_Y(T-t)}$$
$$\times [1 + \bar{c}^{X\to Y}(0, t, T) + \ldots], \quad (24)$$

where the function $\bar{c}^{X\to Y}$ is

$$\bar{c}^{X\to Y}(0, t, T) \equiv \frac{A_{01}^{X\to Y}}{A_{00}^{X\to Y}}(-1)^{T-t}e^{-\Delta m_Y(T-t)}$$
$$\times \left[\frac{1}{2} + \frac{1}{4}(1 - e^{-\Delta m_Y})\right]$$
$$+ \frac{A_{10}^{X\to Y}}{A_{00}^{X\to Y}}(-1)^t e^{-\Delta m_X t}\left[\frac{1}{2} + \frac{1}{4}(1 - e^{-\Delta m_X})\right]$$
$$+ \frac{A_{11}^{X\to Y}}{A_{00}^{X\to Y}}(-1)^T e^{-\Delta m_X t - \Delta m_Y(T-t)}$$
$$\times \left[\frac{1}{2} - \frac{1}{4}(e^{-\Delta m_Y} + e^{-\Delta m_X})\right]. \quad (25)$$

Note that Eq. (25) has the same exponential time dependence as Eq. (22), but with the size of the amplitudes reduced by the factors in square brackets. Thus, the average is equivalent to a smearing that reduces the oscillating state amplitudes. It is possible to compute the Δm_X precisely from fits to two-point correlators. We find values between about 0.2 and 0.4 in lattice units. Given these values, the first two factors in brackets reduce their respective amplitudes by approximately a factor of 2, and the targeted, nonoscillating term is reduced by a factor of ~ 6–10.

Specializing to the $B \to D^*$ case, consider the double ratio

$$R_{A_1}(0, t, T) = \frac{A_{00}^{B\to D^*}A_{00}^{D^*\to B}}{A_{00}^{D^*\to D^*}A_{00}^{B\to B}}[1 + c^{B\to D^*}(0, t, T)$$
$$+ c^{D^*\to B}(0, t, T) - c^{D^*\to D^*}(0, t, T)$$
$$- c^{B\to B}(0, t, T) + \ldots], \quad (26)$$

where we have again factored out the ground state contribution. Equation (26) follows from Eq. (18) treating the c's as small. Note that the c's are expected to be similar in numerator and denominator, and to the extent that they are the same they will cancel in this expression. Applying the average in Eq. (23) directly to the double ratio,
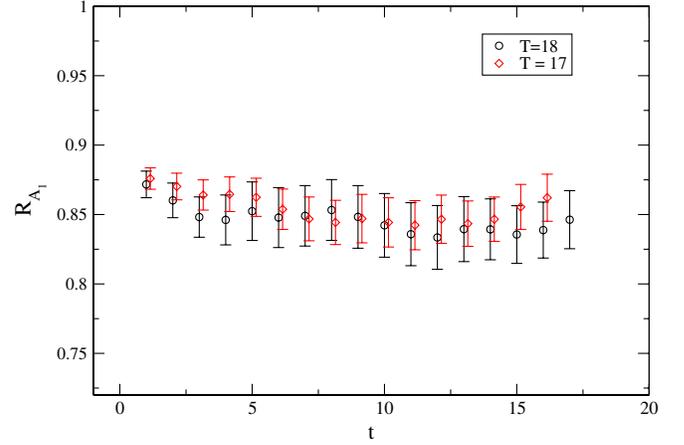

FIG. 1 (color online). Double ratio R_{A_1} on the $a\hat{m}' = 0.0124$ fine ($a = 0.09$ fm) ensemble. The source was fixed to time slice 0, and the operator position was varied as a function of time. Two different sink points were used with even and odd time separations between source and sink in order to study the effect of nonoscillating contributions from wrong parity states.

$$\bar{R}(0, t, T) \equiv \tfrac{1}{2}R(0, t, T) + \tfrac{1}{4}R(0, t, T + 1)$$
$$+ \tfrac{1}{4}R(0, t + 1, T + 1), \quad (27)$$

we get

$$\bar{R}_{A_1}(0, t, T) = \frac{A_{00}^{B\to D^*}A_{00}^{D\to B^*}}{A_{00}^{D\to D^*}A_{00}^{B\to B^*}}[1 + \bar{c}^{B\to D^*}(0, t, T)$$
$$+ \bar{c}^{D\to B^*}(0, t, T) - \bar{c}^{D\to D^*}(0, t, T)$$
$$- \bar{c}^{B\to B^*}(0, t, T) + \ldots], \quad (28)$$

where each of the oscillating state terms in the individual three-point functions is suppressed according to Eq. (25).

Although Δm_B and Δm_{D^*} can be obtained from fits to the two-point correlators, the oscillating state amplitudes
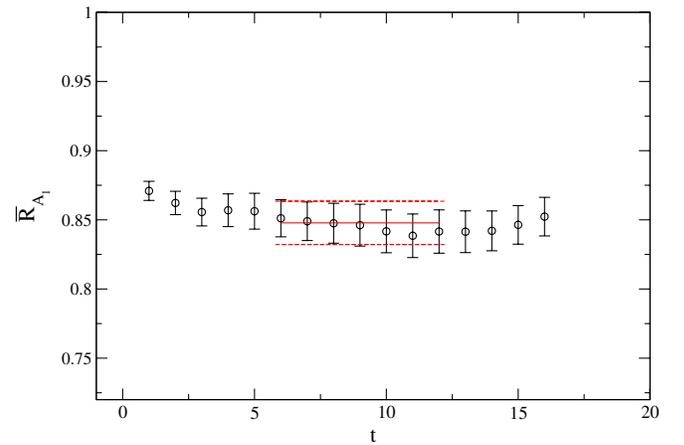

FIG. 2 (color online). Averaged double ratio, $\bar{R}_{A_1}$, of Eq. (27) on the $a\hat{m}' = 0.0124$ fine ($a = 0.09$ fm) ensemble. The plateau fit is shown with 1σ error band.

appearing in the three-point correlators must be determined directly from the three-point correlator data. Figure 1 shows the double ratio R_{A_1} used to obtain $h_{A_1}(1)$. The source is at time slice 0, the sink is at T, and the operator position is varied along t. Two different source-sink separations were generated that differed by a single time unit at the sink ($T = 17, 18$). The average of these two correlators was taken according to Eq. (27), and this average was fit (including the full covariance matrix) to a constant, as shown in Fig. 2. There is no detectable oscillation even before the average is taken, as can be seen in Fig. 1; according to Eq. (25) the oscillating contributions are reduced even further in the average so that their systematic errors can be safely neglected.

IV. PERTURBATION THEORY

Lattice perturbation theory is needed in order to calculate the short-distance coefficient ρ_{A_1} defined in Eq. (19). Although naive lattice perturbation theory appears to converge slowly, the two main causes have been identified [50]: the bare gauge coupling is a poor expansion parameter, and coefficients are large when tadpole diagrams occur. If a renormalized coupling is used as an expansion parameter, and one computes only those quantities for which the tadpole diagrams largely cancel, then lattice perturbation theory seems to converge as well as perturbation theory in continuum QCD.

Only the vertex correction contributes to the ρ factor, as the wave-function renormalization (including all tadpoles) cancels by construction. Even the vertex correction partially cancels, and the one-loop coefficient is found to be small. The perturbative corrections to the ρ factor can be written as

$$\rho_{J_\Gamma}^{hh'} \equiv \frac{Z_{J_\Gamma}^{hh'}}{\sqrt{Z_{V_4}^{hh} Z_{V_4}^{h'h'}}} = 1 + \alpha_V(q^*) 4\pi \rho_{J_\Gamma}^{hh'[1]} + \dots, \quad (29)$$

where $\rho_{J_\Gamma}^{hh'[1]}$ is the coefficient of the one-loop correction, and the coupling α_V is the renormalized strong coupling constant in the V scheme [50,62], which is based on the static-quark potential. The coupling is determined following the procedure of Ref. [63]. The scale q^* of the running coupling $\alpha_V(q^*)$ should be chosen to be the typical momentum of a gluon in the loop. A prescription for calculating this scale was introduced by Brodsky, Lepage, and Mackenzie [50,62]. They defined q^* by

$$\ln(q^{*2}) = \frac{\int d^4 q f(q) \ln(q^2)}{\int d^4 q f(q)}, \quad (30)$$

where $f(q)$ is the one-loop integrand and the numerator is the first log moment. This prescription was extended by Hornbostel, Lepage, and Morningstar (HLM) [64] to cases where the one-loop contribution is anomalously small leading to a break down of Eq. (30). The HLM prescription

TABLE III. Computed values of ρ_{A_1} in the HLM prescription [64]. The first three columns label each ensemble with the approximate lattice spacing in fm, the light sea quark mass $a\hat{m}'$, and the strange quark mass am'_s. The fourth column is aq^*_{HLM}, where the error is calculated using the statistical error from VEGAS for the 0th, 1st, and 2nd moments of the one-loop integrals. The fifth column is ρ_{A_1} on that ensemble, and the errors are the statistical errors from the VEGAS evaluation, including the one-loop coefficients and q^*_{HLM}.

a (fm)	$a\hat{m}'$	am'_s	aq^*_{HLM}	ρ_{A_1}
0.15	0.0194	0.0484	2.03(10)	0.9966(2)
0.15	0.0097	0.0484	2.03(10)	0.9966(2)
0.12	0.02	0.05	1.96(10)	0.9964(2)
0.12	0.01	0.05	1.96(10)	0.9964(2)
0.12	0.007	0.05	1.96(10)	0.9964(2)
0.12	0.005	0.05	1.96(10)	0.9964(2)
0.09	0.0124	0.031	2.98(14)	1.00298(9)
0.09	0.0062	0.031	2.98(14)	1.00300(9)
0.09	0.0031	0.031	2.98(14)	1.00301(9)

for q^* takes into account two-loop contributions to the gluon propagator via the inclusion of second log moments. Since we do encounter anomalously small one-loop corrections in ρ_{A_1}, the HLM prescription was used to determine q^*. Results for q^*_{HLM} and ρ_{A_1} needed for this calculation are given in Table III. The ρ factor varies somewhat as a function of lattice spacing, and is even slightly different from ensemble to ensemble at the same nominal lattice spacing, due to the slightly different β values used to generate the gauge fields.

The calculation of ρ_{A_1} is described in Refs. [65,66]. It uses automated perturbation theory techniques to generate the Feynman rules and VEGAS [67] for the numerical integration of the loop integrals. As a check, it was verified that this calculation reproduces known results for the heavy-heavy currents with the Wilson plaquette action [29] and for the V_4 current in the massless limit with the Symanzik improved gauge action.

As mentioned in the introduction, we have exploited the ρ factor to implement a blind analysis. Two of us applied a multiplicative offset close to 1 to the ρ factor, generated with a random key. The offset was not unlocked until the procedure for determining the systematic errors in the rest of the analysis had been finalized.

V. STAGGERED CHIRAL PERTURBATION THEORY

The simulation masses $\hat{m}'_{\text{val}}$ and $\hat{m}'_{\text{sea}}$ (for valence and sea) are all larger than the physical $\hat{m}$. A controlled chiral extrapolation can be guided by an appropriate chiral effective theory that includes the effect of staggered-quark discretization errors. Rooted staggered chiral perturbation theory (rSχPT), which has been formulated for heavy-light quantities in Ref. [68], is such a theory. In rSχPT, a replica

method is used to take into account the effect of rooting; this procedure has been justified in Refs. [33,69].

Because of taste-symmetry breaking, the staggered theory has 16 light pseudoscalar mesons instead of 1. The tree-level relation for the masses of light staggered mesons in the chiral theory is [17,18]

$$m^2_{xy,\Xi} = \mu_0(m_x + m_y) + a^2\Delta_\Xi, \qquad (31)$$

where m_x and m_y are staggered-quark masses, μ_0 is the continuum low-energy constant, and $a^2\Delta_\Xi$ are the splittings of the 16 pions of taste Ξ. For staggered quarks there exists a residual SO(4) taste symmetry broken at $\mathcal{O}(a^2)$, such that there is some degeneracy among the 16 pions [17], and the taste index Ξ runs over the multiplets P, A, T, V, I with degeneracies 1, 4, 6, 4, 1. The splitting $a^2\Delta_P$ vanishes because there is an exact (nonsinglet) lattice axial symmetry.

Schematically, the next-to-leading-order (NLO) result for the relevant form factor is

$$h^{\rm NLO}_{A_1}(1)/\eta_A = 1 + X_A(\Lambda_\chi) + \frac{g^2_{DD^*\pi}}{48\pi^2 f^2} \times \log_{s 1-\rm loop}(\Lambda_\chi), \qquad (32)$$

where $X_A(\Lambda_\chi)$ is a low-energy constant of the chiral effective theory, and is therefore independent of light-quark mass and cancels the chiral scale dependence Λ_χ of the chiral logarithms. By heavy-quark symmetry, $X_A(\Lambda_\chi)$ is proportional to $1/m_c^2$ in the heavy-quark expansion. The term η_A is a factor that matches heavy-quark effective theory to QCD, and contains perturbative-QCD logarithmic dependence on the heavy-quark masses; it is independent of light-quark mass. The term proportional to $g^2_{DD^*\pi}$ is shorthand for the one-loop staggered chiral logarithms, and is given in the appendix for ease of reference. The rooted staggered expression was derived in Ref. [22]. The one-loop staggered logarithms depend on both valence and sea quark masses, and include taste-breaking effects coming from the light-quark sector. This expression also contains explicit dependence on the lattice spacing a, and requires as inputs the parameters of the staggered chiral Lagrangian δ'_V, δ'_A, in addition to the staggered taste splittings $\Delta_{P,A,T,V,I}$ [16]. These parameters can be obtained from chiral fits to the light pseudoscalar meson sector and are held fixed in the chiral extrapolation of $h_{A_1}(1)$. The continuum low-energy constant $g_{DD^*\pi}$ appears, and below we take a generous range inspired by a combined fit to many different experimental inputs, including a leading-order analysis of the D^* width. The D^*-D splitting $\Delta^{(c)}$ is well determined from experiment. The only other parameter that appears at NLO is the constant $X_A(\Lambda)$, and this is determined by our lattice data for $h_{A_1}(1)$.

Although the lattice data are well described by the NLO formula, it is useful to go beyond NLO and to include the next-to-next-to-leading-order (NNLO) analytic terms as a

way to estimate systematic errors. We do not include the NNLO logarithms because they are unknown and would require a two-loop calculation. The expression including analytic terms through NNLO is

$$h^{\rm NNLO}_{A_1}(1)/\eta_A = 1 + {\rm NLO} + c_1 m^2_{X_P} + c_2(2m^2_{U_P} + m^2_{S_P}) + c_3 a^2, \qquad (33)$$

where the subscript P on the meson masses indicates the taste pseudoscalar mass. We use the notation from the rSχPT literature that m_{X_Ξ} is a taste Ξ meson made of two valence x quarks, m_{U_Ξ} is a taste Ξ meson made of two light sea quarks, and m_{S_Ξ} is a taste Ξ meson made of two strange sea quarks. By heavy-quark symmetry, the c_i are suppressed by a factor of $1/m_c^2$. Since the only free parameter through NLO is an overall constant, we include the NNLO analytic terms in the fit used for our central value. This leads to a larger statistical error and is more conservative.

VI. TREATMENT OF CHIRAL EXTRAPOLATION

In this section, we discuss the approach we have developed to disentangle the heavy- and light-quark discretization effects and to perform the chiral and continuum extrapolations. In the Fermilab method, heavy-quark discretization errors can be estimated by comparing the heavy-quark expansions for lattice gauge theory and continuum QCD [28–30,70]. The dependence on a is not simply a power series (unless $ma \ll 1$), so power-counting estimates in HQET are used. On the other hand, some of the light-quark discretization effects are constrained by rSχPT. The heavy-quark errors are asymptotically constrained by the Symanzik low-energy Lagrangian when $m_h a \ll 1$ and by heavy-quark symmetry even when $m_h a$ is close to 1. In the region in between, the errors smoothly interpolate the asymptotic behavior [49,70]. The errors in the SW action used for the heavy quarks decrease with lattice spacing as $\alpha_s a$ in the $m_h a \ll 1$ region, as compared with the light-quark (improved staggered) discretization errors, which decrease much faster, as $\alpha_s a^2$.

The first step of the method is to normalize the numerical data for $h_{A_1}(1)$ to a fiducial point by forming the ratio

$$\mathcal{R}_{\rm fid}(m_x, \hat{m}', m'_s, a) \equiv \frac{h_{A_1}(m_x, \hat{m}', m'_s, a)}{h_{A_1}(m^{\rm fid}_x, \hat{m}^{\rm fid}, m^{\rm fid}_s, a)}, \qquad (34)$$

where $m^{\rm fid}$ is a fiducial mass, m_x is the light (spectator) valence quark, $\hat{m}'$ is the isospin averaged light sea quark on a particular ensemble, and m'_s is the strange sea quark on that ensemble. (Note that the factor of η_A in Eqs. (32) and (33) cancels in the ratio.) The principle advantage of this ratio is that heavy-quark discretization effects largely cancel, since the heavy quarks are the same in numerator and denominator. This allows us to disentangle the heavy-quark discretization effects from those of the light-quark

sector coming from staggered chiral logarithms, thus isolating the (taste-violating) discretization effects specific to the staggered light quarks. These light-quark discretization effects can appear in nonanalytic terms in rSχPT and are due to violations of taste symmetry. They can be removed to a given order in rSχPT (we work to NLO) in fits to the numerical data at multiple lattice spacings using the explicit rSχPT formula of Eq. (33), since this formula includes the staggered lattice artifacts. The continuum limit of the ratio $\mathcal{R}_{\text{fid}}$ can be obtained using our fitted values for parameters in rSχPT and taking $a \rightarrow 0$ in the rSχPT expression for $\mathcal{R}_{\text{fid}}$. We do not need a more explicit ansatz for the functional form of the heavy-quark discretization effects, since they largely cancel in the ratio.

Normalizing the continuum extrapolated ratio $\mathcal{R}_{\text{fid}}$ by h_{A_1} at the fiducial point on a very fine fiducial lattice where the heavy-quark discretization effects are small gives a value close to the physical continuum result,

$$
\begin{aligned}
h_{A_1}(\hat{m}, \hat{m}, m_s, 0) &\approx h_{A_1}(m_x^{\text{fid}}, \hat{m}^{\text{fid}}, m_s^{\text{fid}}, a^{\text{fid}}) \\
&\times \mathcal{R}_{\text{fid}}(\hat{m}, \hat{m}, m_s, 0),
\end{aligned} \tag{35}
$$

where the relation becomes exact as $a^{\text{fid}} \rightarrow 0$. Note that the requirement that the heavy-quark discretization effects must be small enforces the condition that the improved staggered light-quark discretization effects be even smaller (and likely negligible) because the staggered discretization effects decrease much faster with lattice spacing. The fiducial masses m_x^{fid}, $\hat{m}^{\text{fid}}$, and m_s^{fid} should be chosen large enough that it would be feasible to simulate this mass point on a very fine lattice (since the cost rises significantly as the mass of the light sea quarks is decreased), thus normalizing the lattice data to a point where the heavy-quark discretization effects are small. The fiducial masses should not be chosen so large, however, that rSχPT would not be a reliable guide in performing the continuum and chiral extrapolation of $\mathcal{R}_{\text{fid}}$. This method can be considered the crudest form of step scaling, but it does illustrate that one does not need lattices, which are simultaneously fine enough for b quarks and large enough for light quarks in order to simulate, with high precision, quantities that involve both. In practice, we find $m_x^{\text{fid}} = \hat{m}^{\text{fid}} \approx 0.4 m_s$ and $m_s^{\text{fid}} \approx m_s$ are reasonable values for the fiducial masses. The fiducial lattice spacing should be chosen as fine as is practical; a succession of progressively finer fiducial lattices would be desirable for verifying that the a dependence is of the expected size. In this work we take our finest lattice (0.09 fm) as the fiducial lattice, but we apply Eq. (35) with the coarser lattices taken as fiducial lattices in order to estimate discretization errors. We note that the method presented above can be applied to all calculations involving the Fermilab treatment of heavy quarks and staggered light quarks, not only the $B \rightarrow D^* \ell \nu$ form factor h_{A_1}. It may also be desirable to compute quantities at the fiducial point (or a succession of such points) using an even

further improved action for the heavy quarks. Once the fiducial lattice spacing is of the order 0.03–0.01 fm, even the bottom quark may be treated as a "light" quark with the highly improved staggered action [71] or with chiral fermions, for which mass dependent discretization effects are small. Conserved currents could then be used for many simple heavy-light quantities, removing the need for a perturbative renormalization.

For the chiral extrapolation of h_{A_1} we find it useful to form two additional ratios

$$
\mathcal{R}_{\text{sea}}(\hat{m}', m_s', a) \equiv \frac{h_{A_1}(m_x^{\text{fid}}, \hat{m}', m_s', a)}{h_{A_1}(m_x^{\text{fid}}, \hat{m}^{\text{fid}}, m_s^{\text{fid}}, a)}, \tag{36}
$$

$$
\mathcal{R}_{\text{val}}(m_x, \hat{m}', m_s', a) \equiv \frac{h_{A_1}(m_x, \hat{m}', m_s', a)}{h_{A_1}(m_x^{\text{fid}}, \hat{m}', m_s', a)}, \tag{37}
$$

whose product is clearly $\mathcal{R}_{\text{fid}}$, Eq. (34). $\mathcal{R}_{\text{sea}}$ and $\mathcal{R}_{\text{val}}$ separate the sea and valence quark mass dependence, which makes it easier to assess systematic errors. The values of h_{A_1} that enter Eqs. (36) and (37) are obtained from

$$
h_{A_1} = \rho \sqrt{\bar{R}_{A_1}}, \tag{38}
$$

where $\bar{R}_{A_1}$ is the average of double ratios defined in Eq. (28). The ratios in Eqs. (36) and (37) are now quadruple ratios, where the excited-state contamination is further suppressed over that of the double ratio. Performing the chiral extrapolation, taking the continuum limit of the two ratios, and multiplying them together we recover $\mathcal{R}_{\text{fid}}(\hat{m}, \hat{m}, m_s, 0)$ by construction. Thus, we can rewrite Eq. (35) as

$$
\begin{aligned}
h_{A_1}^{\text{phys}} &\approx h_{A_1}(m_x^{\text{fid}}, \hat{m}^{\text{fid}}, m_s^{\text{fid}}, a^{\text{fid}}) \\
&\times [\mathcal{R}_{\text{sea}}(\hat{m}, m_s, 0) \times \mathcal{R}_{\text{val}}(\hat{m}, \hat{m}, m_s, 0)], \tag{39}
\end{aligned}
$$

where, again, the relation becomes exact as $a^{\text{fid}} \rightarrow 0$.

To the extent that the extrapolation in sea quark masses is mild, the ratio $\mathcal{R}_{\text{sea}}$ should be close to 1, since the valence light mass is the same in both numerator and denominator. $\mathcal{R}_{\text{val}}$ contains less trivial chiral behavior. However, since the numerator and denominator are computed on the same ensemble (with different valence masses), they are correlated, and statistical errors tend to cancel in $\mathcal{R}_{\text{val}}$. The ratio $\mathcal{R}_{\text{sea}}$ has small statistical errors because the valence mass m_x^{fid} in that ratio is relatively heavy. Of course, the heavy-quark discretization errors are significantly suppressed in both ratios, isolating the light-quark mass dependence and staggered discretization effects. A direct chiral fit to the numerical data (not involving the ratios introduced here) would require a more explicit

TABLE IV. Fiducial masses used at the three different lattice spacings. The first four columns are the approximate lattice spacing in fm, the fiducial valence quark mass, the fiducial light sea quark mass, and the fiducial strange quark mass. The fifth and sixth columns are the values of $\sqrt{\bar{R}_{A_1}}$ and $h_{A_1}^{\text{fid}}$, respectively, computed at that fiducial point.

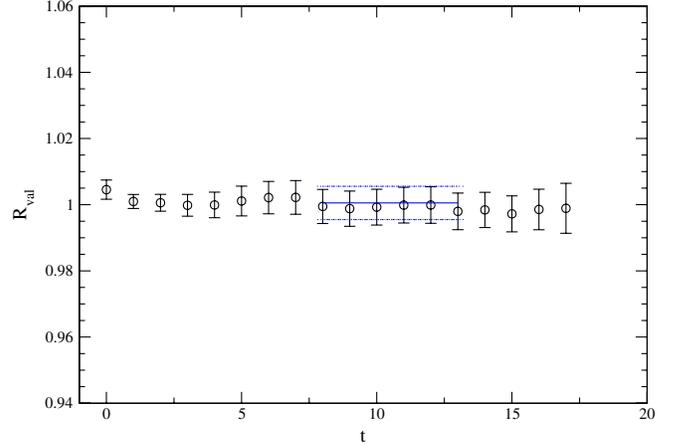| Lattice spacing (fm)	am_x^{fid}	$a\hat{m}^{\text{fid}}$	am_s^{fid}	$\sqrt{\bar{R}_{A_1}}$	$h_{A_1}^{\text{fid}}$
0.15	0.0194	0.0194	0.0484	0.9211(73)	0.9180(73)
0.12	0.02	0.02	0.05	0.9112(73)	0.9079(73)
0.09	0.0124	0.0124	0.031	0.9210(85)	0.9237(85)

FIG. 3 (color online). $\mathcal{R}_{\text{val}}$ on the $a\hat{m}' = 0.0062$ fine ensemble. The valence mass in the numerator is the full QCD value of $am_x' = 0.0062$ while the fiducial valence mass in the denominator is $am_x^{\text{fid}} = 0.0124$. The fit to a constant has a $\chi^2/\text{d.o.f} = 0.20$.

ansatz for the treatment of the heavy-quark discretization effects than is needed in the ratio fits.[2] Note that in the ratios the fiducial point need not be tuned to the same mass at every lattice spacing; differences can be accounted for in the fit itself. The fiducial points used at different lattice spacings are $m_x^{\text{fid}} = \hat{m}^{\text{fid}} = 0.4m_s'$ and $m_s^{\text{fid}} = m_s'$. The explicit values are given in Table IV, along with the calculated values of $\sqrt{\bar{R}_{A_1}}$ and $h_{A_1}^{\text{fid}}$ at that fiducial point.

The constant term $X_A(\Lambda_\chi)$ in Eq. (32) cancels in the ratios $\mathcal{R}_{\text{sea}}$ and $\mathcal{R}_{\text{val}}$, so the behavior of these ratios is completely predicted through NLO in the chiral expansion. We find good agreement between the predicted form and the numerical data. However, given that our fiducial spectator quark mass is rather large (around $0.4m_s$), we include the NNLO analytic terms in the ratio fits in order to estimate systematic errors associated with the chiral expansion. There are only two new continuum low-energy constants introduced at this higher order, and the ratios $\mathcal{R}_{\text{sea}}$ and $\mathcal{R}_{\text{val}}$ determine one each. There is also an analytic term proportional to a^2 appearing at this order, but it cancels in each of the $\mathcal{R}_{\text{sea}}$ and $\mathcal{R}_{\text{val}}$ ratios.

In future calculations, it would be feasible to use a much finer lattice spacing for the fiducial point, thereby further reducing heavy-quark discretization errors. For now, however, we use $h_{A_1}(m_x^{\text{fid}}, \hat{m}^{\text{fid}}, m_s^{\text{fid}}, 0.09 \text{ fm})$, with the fiducial masses in Table IV, in Eq. (39). As a way to estimate discretization errors we use our results for $h_{A_1}^{\text{fid}}$ at the two coarser lattice spacings in Eq. (39) also.

At the lattice spacings used in this work the light-quark discretization effects may still be non-negligible compared with heavy-quark discretization effects. With rSχPT it is possible to remove from $h_{A_1}^{\text{fid}}$ the discretization effects associated with staggered chiral logarithms, although purely analytic discretization errors remain. Removing this subset of staggered effects leads to a value for the

fiducial form factor, which we call the "taste-violations-out" value. Not removing them leads to the "taste-violations-in" value. The difference turns out to be negligible, less than 0.1% on our coarsest ensemble and less than 0.01% on the fine ensemble. Thus, the discretization effects in our lattice data coming from taste violations in the staggered chiral logarithms are extremely small at the fiducial point mass, and we neglect this difference in the analysis.

Figure 3 shows the plateau fit to the ratio $\mathcal{R}_{\text{val}}$ on the fine ensemble with $(a\hat{m}', am_s') = (0.0062, 0.031)$. The valence mass in the numerator is the full QCD value of $am_x' = 0.0062$, while the fiducial valence mass in the denominator is $am_x^{\text{fid}} = 0.0124$. Both numerator and denominator are computed on the same ensemble, so they have the same sea quark masses, and correlated statistical errors largely cancel in the ratio, as expected. Excited-state contamination is also reduced. Computed values for $\mathcal{R}_{\text{sea}}$ on all of our ensembles are given in Table V, and the computed values for $\mathcal{R}_{\text{val}}$ are given in Table VI.

TABLE V. Computed values of $\mathcal{R}_{\text{sea}}$. The first three columns are the arguments of $\mathcal{R}_{\text{sea}}$ as defined in Eq. (36); they are the light sea quark mass $\hat{m}'$, the strange quark mass m_s', and the approximate lattice spacing in fm. The fourth column is $\mathcal{R}_{\text{sea}}$.

$a\hat{m}'$	am_s'	a (fm)	$\mathcal{R}_{\text{sea}}$
0.0097	0.0484	0.15	1.009(12)
0.01	0.05	0.12	1.0070(98)
0.007	0.05	0.12	1.0027(91)
0.005	0.05	0.12	1.014(10)
0.0062	0.031	0.09	1.000(12)
0.0031	0.031	0.09	0.996(10)

---

[2]A direct (correlated) chiral fit would still, however, reflect the correlations, which cause cancellations in the statistical errors in the ratios.

TABLE VI. Computed values of $\mathcal{R}_{\text{val}}$. The first four columns are the arguments of $\mathcal{R}_{\text{val}}$ as defined in Eq. (37); they are the light valence quark mass m_x, the light sea quark mass $\hat{m}'$, the strange quark mass m'_s, and the approximate lattice spacing in fm. The fifth column is $\mathcal{R}_{\text{val}}$.

am_x	$a\hat{m}'$	am'_s	a (fm)	$\mathcal{R}_{\text{val}}$
0.0097	0.0097	0.0484	0.15	1.0056(65)
0.01	0.01	0.05	0.12	0.9994(41)
0.007	0.007	0.05	0.12	0.9900(57)
0.005	0.005	0.05	0.12	1.0081(90)
0.0062	0.0062	0.031	0.09	1.0005(50)
0.0031	0.0031	0.031	0.09	1.0043(62)

VII. SYSTEMATIC ERRORS

In the following subsections, we examine the uncertainties in our calculation due to fitting and excited states, the heavy-quark mass dependence, the chiral extrapolation of the light spectator quark mass, discretization errors, and perturbation theory. As mentioned in Sec. II, statistical uncertainties are computed with a single elimination jackknife and the full covariance matrix.

A. Fitting and excited states

We have examined plateau fits to the time dependence of the double and quadruple ratios introduced in Secs I and V. The χ^2 in our fits is defined with the full covariance matrix. The fits to the ratios were done under a single elimination jackknife, after blocking the numerical data by 8 on the fine lattices and by 4 on the coarse and coarser lattices. The blocking procedure averages 4 (or 8) successive configurations before performing the single elimination jackknife. These values for the block size were chosen such that the statistical error on the double ratio fit did not increase when a larger block size was used. Statistical errors were determined in fits that included the full correlation matrix, which was remade for each jackknife fit. The jackknife data sets on different ensembles were then combined into a larger block-diagonal jackknife data set in order to perform the chiral fits. In this way, the fully correlated statistical errors were propagated through to the final result.

With our high statistics (several hundred lattice gauge field configurations for each ensemble), we are able to resolve the full covariance matrix well enough that we do not need to apply a singular value decomposition cut on the eigenvalues of the covariance matrix. The double ratio fit is needed to establish $h_{A_1}(1)$ at the fiducial point (which was computed on the 0.0124/0.031 fine ensemble), while the quadruple ratios, $\mathcal{R}_{\text{val}}$ and $\mathcal{R}_{\text{sea}}$ are computed on the other ensembles in order to perform the chiral extrapolation and to remove taste-breaking nonanalytic terms. We find that the fit to the double ratio at the fiducial point on the 0.0124/0.031 ensemble is well described by a constant over a range of seven time slices. The excited-state con-

tamination in the quadruple ratios is even further suppressed, and we find that the correlated χ^2 values allow for a constant fit region of six to ten time slices, depending upon the lattice spacing. We take the good correlated $\chi^2/\text{d.o.f.}$, ranging from 0.15 to 1.00, in our constant plateau fits as evidence that the excited-state contamination in these fits is negligible as compared with other errors.

As an additional check of the jackknife fitting procedure, bootstrap fits were done to all of the double and quadruple ratios needed for this work. Close agreement was found for both central values and statistical errors. The statistical errors were typically the same size within 10%, and central values were well within 1σ. The jackknife procedure had slightly larger errors than that of the bootstrap.

B. Heavy-quark mass dependence

The value for $h_{A_1}(1)$ depends on the heavy-quark masses, which are set by tuning the hopping parameters κ_b and κ_c. The principal method starts by fitting the lattice pole energy to $E(\mathbf{p})$ to the dispersion relation

$$E(\mathbf{p}) = M_1 + \frac{\mathbf{p}^2}{2M_2} + b_1 \mathbf{p}^4 + b_2 \sum_{j=1}^{3} |p_j|^4 + \cdots, \quad (40)$$

in order to obtain the kinetic mass M_2 (as well as b_1 and b_2, which are unimportant here). In the Fermilab method [28,30,49], κ is adjusted so that the kinetic mass agrees with experiment. Here we take the spin-average of kinetic masses of pseudoscalar and vector heavy-strange mesons and obtain our central values for κ_b or κ_c, respectively, from the (spin-averaged) $B_s^{(*)}$ and $D_s^{(*)}$ masses. Applying this procedure we find statistical and fitting errors of 5.6% for κ_b and 1.2% for κ_c on the fine ($a = 0.09$ fm) ensembles. There is an additional error in κ due to discretization effects. We determine this error by estimating the size of discretization effects for the Fermilab action (at $a = 0.09$ fm) as in Ref. [72]. This error is 1.3% for κ_b and 0.3% for κ_c. Adding in quadrature the statistical and fitting error together with the discretization error leads to a total relative uncertainty of 5.7% for κ_b and 1.2% for κ_c. This error budget is summarized in Table VII. Note that these errors are conservative and are likely to decrease substantially with more sophisticated fitting methods and the higher statistics data set currently being generated.

We have computed $h_{A_1}(1)$ at several different values of the bare charm and bottom quark masses, and these simu-

TABLE VII. Errors in the $\kappa_{b,c}$ parameters. The first column labels the heavy quark, the second gives the statistical and fitting error for the κ parameter, the third gives the discretization error, and the fourth combines these in quadrature.

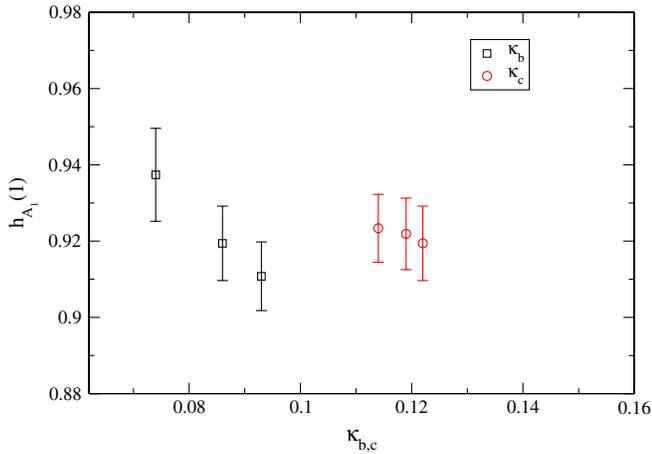| κ	Statistics + fitting	Discretization	Total
κ_c	1.2%	0.3%	1.2%
κ_b	5.6%	1.3%	5.7%

FIG. 4 (color online). $h_{A_1}(1)$ for different κ_h values on the coarse $\hat{m}' = 0.02$ ensemble (full QCD point). The points labeled κ_b show how $h_{A_1}(1)$ depends on κ_b when κ_c is fixed to its tuned value. For the points labeled κ_c the roles of κ_b and κ_c are reversed.

lated points can be used to estimate the error in $h_{A_1}(1)$ from the above uncertainties in the tuning of the heavy-quark κ values. Figure 4 illustrates the dependence of $h_{A_1}(1)$ as a function of bottom and charm quark κ values on one of the coarse ($a = 0.12$ fm) ensembles. The points labeled κ_b show $h_{A_1}(1)$ where we have fixed κ_c to the tuned charm value, but vary the bare κ_b along the x axis. The points labeled κ_c are similar, where the value of κ_b is fixed at its tuned value, and the bare κ_c is varied. The above uncertainties in the κ's, combined with the variation of $h_{A_1}(1)$ with κ, lead to a systematic error of 0.7% in $h_{A_1}(1)$, labeled "kappa tuning" in Table X.

C. Perturbation theory

The perturbative calculation of ρ_{A_1} is needed to match the heavy-quark lattice current, and the calculation has been carried out to one-loop order [$O(\alpha_s)$]. As discussed in Sec. IV, much of the renormalization cancels when forming the ratios of Z factors that define ρ [Eq. (29)], and the coefficients of the perturbation series are small, by construction. The one-loop correction is quite small, only 0.3–0.4% on the different lattice spacings. We take the entire one-loop correction of 0.3% on the fine lattices as an estimate of the error introduced by neglecting higher orders in the perturbative expansion.

D. Chiral extrapolation

We estimate our systematic error due to the chiral extrapolation by comparing fits with and without the additional terms with coefficients c_i in Eq. (33), i.e. analytic terms of higher order than NLO in rSχPT, since the two-loop NNLO logarithms are unknown. We also compare with continuum χPT, both NLO and (partial) NNLO.

There are additional errors due to the uncertainties in the parameters that enter the NLO rSχPT formulas. By far the largest uncertainty of this kind is that due to the uncertainty in $g_{DD^*\pi}$. Finally, there is an error due to a mistuning of the parameter u_0 on the coarse lattices. All of these errors are discussed below in more detail. In the discussion of chiral extrapolation errors, it is important to keep in mind that the chiral logarithms (either rSχPT or continuum) are tiny ($\sim 3 \times 10^{-3}$) in the region where we have data. Nonanalytic behavior is important only near the physical pion mass where the χPT should be a very good description in the continuum. The main feature of the chiral extrapolation is a cusp that appears close to the physical pion mass (in the valence sector), due to the $D\pi$ threshold and the fact that the D-D^* splitting is very close to the physical pion mass. This cusp represents real physics, and must be included in any version of the chiral extrapolation used to estimate systematic errors.

We extrapolate the light sea and light valence quark masses from the values used in the simulations, between $m_s/2$ and $m_s/10$, to the average physical light-quark mass, around $m_s/27$. We use staggered chiral perturbation theory and the prescription introduced in Sec. VI to remove the nonanalytic taste-breaking discretization effects coming from the staggered light-quark sector. Separate fits are performed for the two ratios introduced in Eqs. (36) and (37), $\mathcal{R}_{\mathrm{sea}}$ and $\mathcal{R}_{\mathrm{val}}$. The chiral extrapolation is performed on these ratios, and the staggered discretization errors appearing in the NLO chiral logarithms are removed by taking $a \to 0$ in the rSχPT expression. With the NNLO analytic terms given in Eq. (33) the chiral extrapolation formulas for the ratios are

$$\mathcal{R}_{\mathrm{val}} = 1 + \mathrm{NLO}_{\mathrm{logs}} + c_1 m_{X_P}^2, \qquad (41)$$

$$\mathcal{R}_{\mathrm{sea}} = 1 + \mathrm{NLO}_{\mathrm{logs}} + c_2(2m_{U_P}^2 + m_{S_P}^2), \qquad (42)$$

where $\mathrm{NLO}_{\mathrm{logs}}$ is a schematic notation representing the chiral logarithms coming from numerator and denominator. These terms are different for the two ratios, and can be obtained straightforwardly from the definitions of the ratios Eqs. (36) and (37), and the formula for the nonanalytic terms in Eq. (A1). The formula for $\mathcal{R}_{\mathrm{val}}$ in the continuum is given explicitly in Eq. (A6), for the purposes of illustration. The NNLO term $c_3 a^2$ in Eq. (33) cancels in the ratios, and $\mathcal{R}_{\mathrm{sea}}$ and $\mathcal{R}_{\mathrm{val}}$ each determine one of the remaining two NNLO coefficients. Note that the factor of η_A in Eqs. (32) and (33) cancels in the chiral formulas for the two ratios. The only free parameters in our chiral fits are c_1 and c_2; the rest are determined from phenomenology or from rSχPT fits to the pseudoscalar sector.

The ratios in Eqs. (36) and (37) are completely predicted through NLO in the continuum once f_π, $g_{DD^*\pi}$, and the D-D^* splitting $\Delta^{(c)}$ are taken from experiment. The constants f_π and $g_{DD^*\pi}$ appear in an overall multiplicative
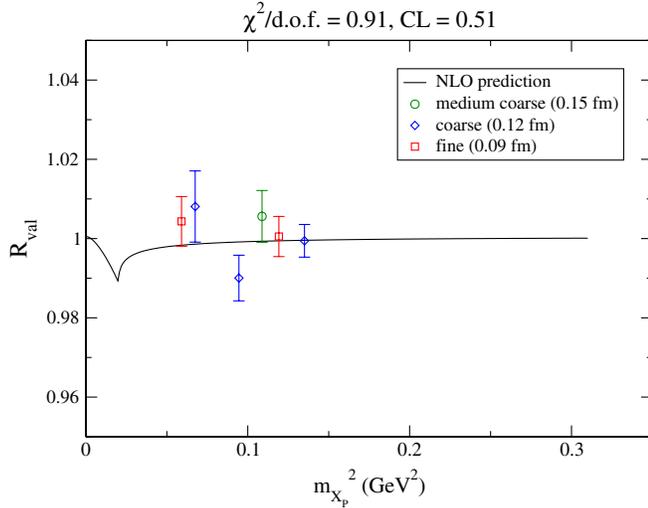
FIG. 5 (color online). $\mathcal{R}_{\text{val}}$ ratio versus valence pion mass squared on all ensembles for the three different lattice spacings. The curve is the continuum prediction through NLO in continuum χPT for this quantity. (See appendix.)
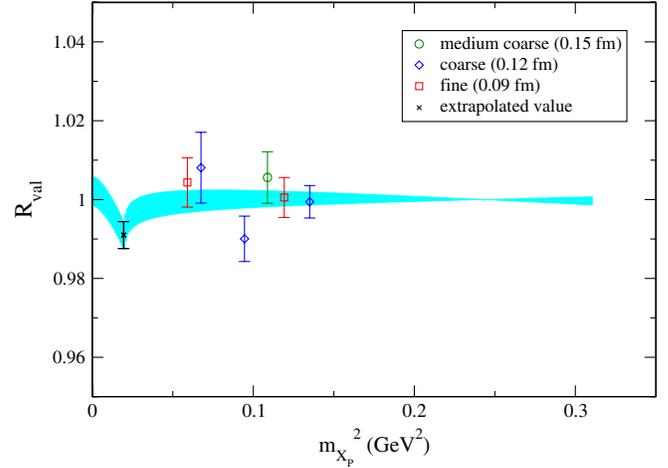

FIG. 6 (color online). $\mathcal{R}_{\text{val}}$ ratio versus valence pion mass squared on all ensembles for the three different lattice spacings. The curve is the fit with 1 sigma error band to the ratio for all three lattice spacings using rSχPT, extrapolated to the continuum by taking $a \to 0$ in the NLO staggered chiral logarithms.

factor $\frac{g^2_{DD^*\pi}}{48\pi^2 f^2_\pi}$ in front of the logarithmic term, as can be seen in Eq. (A1) and (A6). We take a fairly conservative range for the constant $g_{DD^*\pi}$ determined from phenomenology, as discussed below, and the errors in this quantity are accounted for in our final error budget. In the mass region where we have data, the NLO continuum chiral logarithms contribute to $h_{A_1}(1)$ at the $\sim 3 \times 10^{-3}$ level or less. Figure 5 illustrates this, where the NLO continuum χPT prediction Eq. (A6) is plotted over our data points for $\mathcal{R}_{\text{val}}$. We find that the NLO continuum χPT describes the data quite well, giving a $\chi^2/\text{d.o.f.} = 0.91$ and a corresponding CL = 0.51. This result is unchanged in the rSχPT fits; the effects of staggering are negligible in the region where we have data. We include the term proportional to c_1 in Eq. (41) in our fits used to obtain the central value for this quantity, as explained in Sec. V. (Since including a linear term proportional to c_1 increases the statistical error in h_{A_1}, we take our central value and statistical error from this fit to be conservative.) This "partial NNLO" fit also has a good $\chi^2/\text{d.o.f.} = 1.05$, with a corresponding CL = 0.39. The constant linear term is small and consistent with zero [$c_1 = -0.006(15)$]. Figure 6 shows the fit to $\mathcal{R}_{\text{val}}$ versus $m^2_{X_P}$ for all three lattice spacings using the rSχPT formula, Eq. (41).

Although the data for $\mathcal{R}_{\text{val}}$ is consistent with a constant, the cusp appearing close to the physical pion mass is a prediction of NLO χPT and has a physical origin, namely, the D-π threshold, as we have remarked. Thus, any fits used to estimate systematic errors, even those that are somewhat *ad hoc*, such as those including higher-order polynomial terms, must include this cusp. Note that the cusp appears at the physical pion mass (in either SU(3) or SU(2) χPT), and is therefore in a region where χPT is

expected to be a reliable expansion. The cusp is a property of the function $F(m, \Delta^{(c)}/m)$ given in Eq. (A2), and the position of the cusp as a function of $m^2_{X_P}$ is determined by the D-D^* splitting $\Delta^{(c)}$ and the physical pion mass. We take these two quantities from experiment rather than from the lattice, since the experimental uncertainties are much smaller.

We find that with or without the NNLO analytic terms, the χPT (continuum or rooted staggered) describes the lattice data with $\chi^2/\text{d.o.f.}$ close to 1 and correspondingly good confidence levels. We find a confidence level for the fit to $\mathcal{R}_{\text{sea}}$ of 0.76 for the fit that includes NNLO analytic terms. The strictly NLO expression for the lattice ratio $\mathcal{R}_{\text{sea}}$ has no free parameters, but it describes the data with a confidence level of 0.73. Similar fits to $\mathcal{R}_{\text{val}}$ are described above and yield reasonable confidence levels for both types of fits. Since the lattice data do not distinguish between these model fit functions, and the fit using only the NNLO analytic terms is not systematic in the chiral expansion, we assign the difference between the two determinations, which is 0.9%, as the systematic error of leaving out higher-order terms when performing the chiral extrapolation. The final results for $\mathcal{R}_{\text{sea}}$, $\mathcal{R}_{\text{val}}$, and $\mathcal{R}_{\text{fid}}$ are given in Table VIII. The errors are statistical only; note that the strictly NLO values have no free parameters, and therefore no statistical errors. The final value of h_{A_1} still has statistical errors coming from the statistical errors in $h^{\text{fid}}_{A_1}$. The extrapolated results for $\mathcal{R}_{\text{fid}}$ are consistent within the statistical errors of the NNLO fit. Again, we choose for our central value the result from the NNLO extrapolation with its larger errors to be conservative.

The cyan (gray) band in Fig. 6 is the continuum extrapolation with $a \to 0$ in the rSχPT formula. For this quantity,

TABLE VIII. Continuum extrapolated values of $\mathcal{R}_{\text{sea}}$, $\mathcal{R}_{\text{val}}$, $\mathcal{R}_{\text{fid}}$, and $h_{A_1}(1)$ evaluated at the physical quark masses. The first column labels the quantity. The second is the computed value including NNLO analytic terms in the chiral fit. The third is the quantity evaluated in purely NLO χPT, and has no free parameters (once $g_{DD^*\pi}$, f_π and $\Delta^{(c)}$ are taken from phenomenology) in the chiral fit. The final row shows $h_{A_1}(1)$, which includes a statistical error coming from $h_{A_1}^{\text{fid}}$. The numbers are the same to the quoted precision using rSχPT or continuum χPT.

	w/NNLO	Strictly NLO
$\mathcal{R}_{\text{sea}}$	1.0059(90)	0.9983
$\mathcal{R}_{\text{val}}$	0.9910(34)	0.9895
$\mathcal{R}_{\text{fid}}$	0.997(10)	0.9878
$h_{A_1}(1)$	0.921(13)	0.9124(84)

the staggered lattice artifacts affecting the chiral logarithms in h_{A_1} are negligible in the region where we have lattice data, which is due mainly to the small size of the chiral logarithms themselves. This is confirmed by the close agreement between the data points at each lattice spacing and the continuum curve. In fact, if we use continuum χPT to perform the chiral extrapolation, the result is unchanged. The primary difference between the rSχPT expression and the continuum χPT expression is the reduction of the cusp near the physical pion mass in rSχPT, though our lattice data are not near enough to the physical pion mass to demonstrate this effect.

Figure 7 shows the fit to $\mathcal{R}_{\text{sea}}$, extrapolated to the continuum and to the physical strange sea quark mass. Note that this ratio does not produce a cancellation of correlations between numerator and denominator and so has larger statistical errors than $\mathcal{R}_{\text{val}}$. Here again the discretization effects due to staggered logarithms are negligibly small. Since the effects of including staggered discretiza-

tion effects in the chiral logarithms are negligible in the region where we have numerical data, and since the only nontrivial feature in the chiral extrapolation is the cusp near the physical pion mass, which we describe by continuum χPT (our extrapolated curve has $a \rightarrow 0$ in the rSχPT formula and thus reduces to the continuum form), we conclude that staggered taste-violating effects appearing in chiral logarithms are essentially removed in our ratio extrapolations.

Figure 8 shows all of the full QCD points on the three lattice spacings. The curve is the quantity

$$
\begin{aligned}
h_{A_1}^{\text{phys}}(\hat{m}') &\approx h_{A_1}^{\text{fid}}(m_x^{\text{fid}}, \hat{m}^{\text{fid}}, m_s^{\text{fid}}, a^{\text{fid}}) \\
&\times [\mathcal{R}_{\text{sea}}(\hat{m}', m_s, 0) \times \mathcal{R}_{\text{val}}(\hat{m}', \hat{m}', m_s, 0)],
\end{aligned}
\tag{43}
$$

which again becomes an exact relation for the physical form factor when $a^{\text{fid}} \rightarrow 0$. The curve is thus the product of the two continuum extrapolated ratio fits shown in Figs. 6 and 7, times the fiducial point, which we take to be $a\hat{m}^{\text{fid}} = 0.0124$ at the fine lattice spacing (the solid square in Fig. 8). Because this is a full QCD curve, the valence mass m_x equals the light sea mass $\hat{m}'$. The other full QCD points are shown as open symbols in Fig. 8 for comparison, though the fits were performed on the ratios and normalized by the fiducial point at $a\hat{m}^{\text{fid}} = 0.0124$. Note that the curve is already extrapolated in the strange sea quark mass, and so does not perfectly overlap with the $a\hat{m}^{\text{fid}} = 0.0124$ point. As discussed above, when this quan-
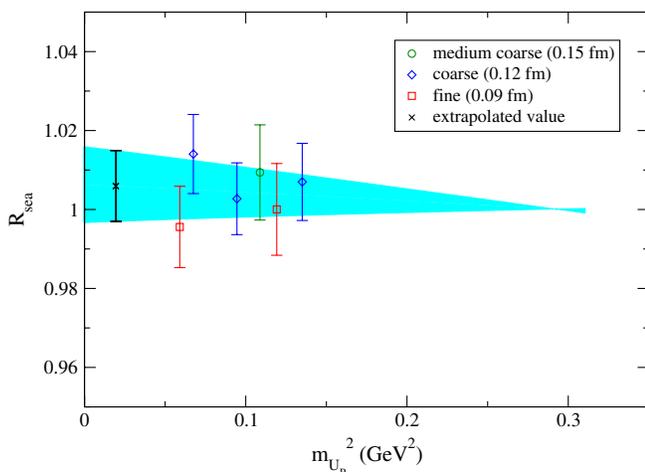

FIG. 7 (color online). $\mathcal{R}_{\text{sea}}$ ratio versus $m_{U_P}^2$ for all ensembles and lattice spacings. The curve is the fit to all of the lattice data, extrapolated to the continuum. The curve is also extrapolated to the physical strange sea quark mass.
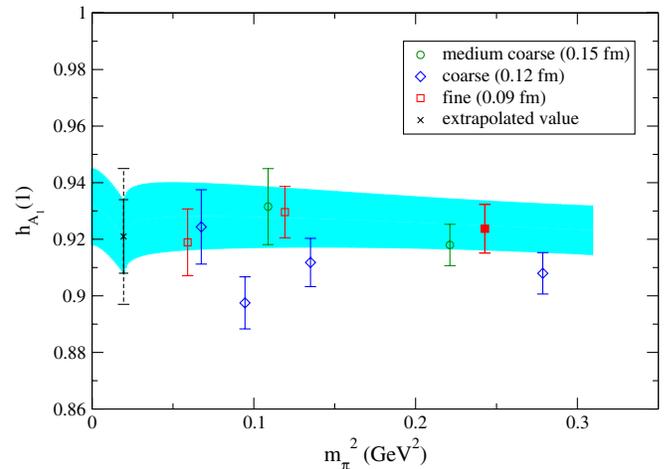

FIG. 8 (color online). The full QCD points versus m_π^2 on the three lattice spacings are shown in comparison to the continuum curve. The curve is the product of the two continuum extrapolated ratio fits shown in Figs. 6 and 7, times the fiducial point, which we have chosen to be the $\hat{m}' = 0.0124$ fine lattice point (the filled square). The curve is already extrapolated to the physical strange sea quark mass, and so does not perfectly overlap with the lattice data point at the fiducial value. The cross is the extrapolated value, where the solid line is the statistical error, and the dashed line is the total systematic error added to the statistical error in quadrature.

tity is evaluated at $\hat{m}' = \hat{m}$ it yields the value of h_{A_1} at physical quark masses. The cross is the extrapolated value, where the solid line is the statistical error, and the dashed line is the total systematic error added to the statistical error in quadrature.

The low-energy constant $g_{DD^*\pi}$ enters the chiral extrapolation formula and determines the size of the cusp near the physical pion mass. Our data do not constrain this constant, so we take a wide range for $g_{DD^*\pi}$ that encompasses the range of values coming from phenomenology and lattice calculations: fits to a wide range of experimental data prior to the measurement of the D^* width by Stewart ($g_{DD^*\pi} = 0.27^{+0.06}_{-0.03}$ [73]), an update of the Stewart analysis including the D^* width ($g_{DD^*\pi} = 0.51$; no error quoted [74]), quark models ($g_{DD^*\pi} \approx 0.38$ [75]), quenched lattice QCD ($g^{N_f=0}_{DD^*\pi} = 0.67 \pm 0.08^{+0.04}_{-0.06}$ [76]), two flavor lattice QCD in the static limit ($g^{N_f=2}_{\text{static}} = 0.516 \pm 0.051$ [77]), and the measurement of the D^* width ($g_{DD^*\pi} = 0.59 \pm 0.07$ [78]). There are as of yet no $2 + 1$ flavor lattice calculations of $g_{DD^*\pi}$. For this work we take $g_{DD^*\pi} = 0.51 \pm 0.2$, leading to a parametric uncertainty of 0.9% in $h_{A_1}(1)$ that is included as a systematic error.

The additional low-energy constants that enter the chiral formulas are the tree-level continuum coefficients μ_0 and f, and the taste-violating parameters that vanish in the continuum. These are the taste splittings $a^2\Delta_\Xi$ with $\Xi = P, A, T, V, I$, and the taste-violating hairpin-coefficients $a^2\delta'_A$ and $a^2\delta'_V$. We set f to the experimental value of the pion decay constant $f_\pi = 0.1307$ GeV in the coefficient of the NLO logarithms. The pion masses used as inputs in the rSχPT formulas are computed from the bare quark masses and converted into physical units using

$$m^2_{xy} = (r_1/r_1^{\text{phys}})^2 \mu_{\text{tree}}(m_x + m_y), \qquad (44)$$

where μ_{tree} is obtained from fits to the light pseudoscalar mass squared to the tree-level form (in r_1 units), $r_1^2 \mu_{\text{tree}}(m_x + m_y)$. This accounts for higher-order chiral corrections and is more accurate than using μ obtained in the chiral limit, giving a better approximation to the pion mass squared at a given light-quark mass. Since the parameters in our lattice simulations at different lattice spacings are expressed in r_1 units, we require the physical value of r_1 to convert to physical units and take the physical pion mass and $\Delta^{(c)}$ from experiment. Thus, the $\approx 2.5\%$ uncertainty in r_1^{phys} gives a parametric error in the chiral extrapolation. Because the chiral extrapolation is so mild, however, this error turns out to be negligible compared with other systematic errors. Since we are taking the pion mass from experiment there is a negligible error due to the light-quark mass uncertainty in the chiral extrapolation. The strange sea quark mass enters the chiral extrapolation formulas, but the dependence is weak, and the error in the bare strange quark mass leads to a negligible parametric error in h_{A_1}. The taste splittings Δ_Ξ have been determined

in Ref. [16], and their approximately 10% uncertainty also leads to a negligible error in $h_{A_1}(1)$. The taste-violating hairpin coefficients have much larger fractional uncertainties, but these too lead to a negligible uncertainty in $h_{A_1}(1)$. Even setting the rSχPT parameters to zero does not change our result for $h_{A_1}(1)$ significantly. As mentioned above, our result does not change if we use the continuum χPT formula in our chiral fits.

In the calculation of the form factor, the tadpole-improved coefficient $c_{\text{SW}} = 1/u_0^3$ is obtained with u_0 from the Landau link on the coarse lattices, but from the plaquette for u_0 on the fine and coarser lattices. Though unintentional, there is nothing wrong with this, since it is not known *a priori* which provides the best estimate of the tadpole improvement factor. However, the u_0 term for the spectator light (staggered) quark, which appears in the tadpole improvement of the Asqtad action, was taken from the Landau link on the coarse lattices, even though the sea quark sector used u_0 from the plaquette. On the fine and coarser lattices, u_0 was taken to be the same in the light valence and sea quark sectors. The estimates of u_0 from plaquette versus Landau link differ only by 4% on the coarse lattices.

Although the effect of this mistuning is expected to be small (correcting u_0 would lead to a slightly different valence propagator and different tuned κ values, thus leading to a small modification of the staggered chiral parameters in the valence sector for the coarse lattices used as inputs to the chiral fit), it is possible to study how much difference it makes using the h_{A_1} lattice data. Including all three lattice spacings and using our preferred chiral fit, we find $h_{A_1}(1) = 0.921(13)$, where the error here is statistical only. If we neglect the coarse data points, we find $h_{A_1}(1) = 0.920(17)$, almost unchanged except for a somewhat larger statistical error. We can also examine the ratios $\mathcal{R}_{\text{val}}$ and $\mathcal{R}_{\text{sea}}$. In our preferred fit to all the lattice data these are 0.9910(34) and 1.0059(90), respectively, where the errors are again only statistical. If we drop the coarse lattice data, these become 0.9960(56) and 0.999(13), respectively. Since the ratio $\mathcal{R}_{\text{sea}}$ has very little valence quark mass dependence, we can combine $\mathcal{R}_{\text{sea}}$ from the fit to all of the lattice data with $\mathcal{R}_{\text{val}}$ from the fit neglecting the coarse lattice data. This is useful, because $\mathcal{R}_{\text{sea}}$ has the larger statistical error, so we would like to use the full lattice data set to determine this ratio, thus isolating the mistuning in the valence sector on the coarse lattices. When this is done we find that the central value of the final $h_{A_1}(1)$ is shifted upward by 0.4%, well within statistical errors and smaller than our other systematic errors. We assign a systematic error of 0.4% due to the u_0 mistuning.

E. Finite volume effects

The finite volume corrections to the integrals which appear in heavy-light χPT formulas, including those for $B \to D^*$ were given by Arndt and Lin [79]. There are no

new integrals appearing in the staggered case, and it is straightforward to use the results of Arndt and Lin in the rSχPT for $h_{A_1}(1)$, as shown in Ref. [22]. We find that although the finite volume corrections in $h_{A_1}(1)$ would be large near the cusp at the physical pion mass on the current MILC ensembles (ranging in size from 2.5–3.5 fm), for the less chiral data points at which we have actually simulated, the finite volume effects are negligible. For all data points in our simulations the finite volume corrections are less than 1 part in 10^4. We therefore assign no error due to finite volume effects.

F. Discretization errors

As shown in Refs. [28–30,49], the matching of lattice gauge theory to QCD is accomplished by normalizing the first few terms in the heavy-quark expansion. This is done by tuning the kinetic masses of the D_s and B_s mesons computed using the SW action (for the heavy quarks) to the experimental meson masses. Tree-level tadpole-improved perturbation theory is used to tune the coupling c_{SW} and the rotation coefficient d_1 for the bottom and charm quarks. Once this matching is done, the discretization errors in $h_{A_1}(1)$ are of order $\alpha_s(\bar{\Lambda}/2m_Q)^2$ and $(\bar{\Lambda}/2m_Q)^3$ [28], where the powers of two are combinatoric factors. The leading matching uncertainty is of the order $\alpha_s(\bar{\Lambda}/2m_c)^2$. We estimate the size of this error setting $\alpha_s = 0.3$, $\bar{\Lambda} = 500$ MeV, and $m_c = 1.2$ GeV, which gives $\alpha_s(\bar{\Lambda}/2m_c)^2 = 0.013$.

Since we have numerical data at three lattice spacings we are able to study how well the power-counting estimate accounts for observed discretization effects. Making use of Eq. (43), but varying the fiducial lattice spacing from our lightest to coarsest lattices, we are able to obtain $h_{A_1}(1)$ at physical quark masses, with discretization effects associated with the staggered chiral logarithms removed in the ratios appearing in Eq. (43). The discretization effects that remain are: taste violations in $h_{A_1}^{\text{fid}}$, taste violations at higher order than NLO in the ratios, the effect of the analytic term coming from light-quark discretization effects (proportional to $\alpha_s a^2$), and the heavy-quark discretization effects. The taste violations in $h_{A_1}^{\text{fid}}$ and the taste violations in the ratios appearing at higher order than NLO have been shown to be negligible. We now consider the remaining

TABLE IX. $h_{A_1}(1)$ at physical quark masses at different lattice spacings, where taste-violating effects have been removed, or shown to be negligible. Discretization effects due to analytic terms associated with the light-quark sector and heavy-quark discretization effects remain in the lattice data.

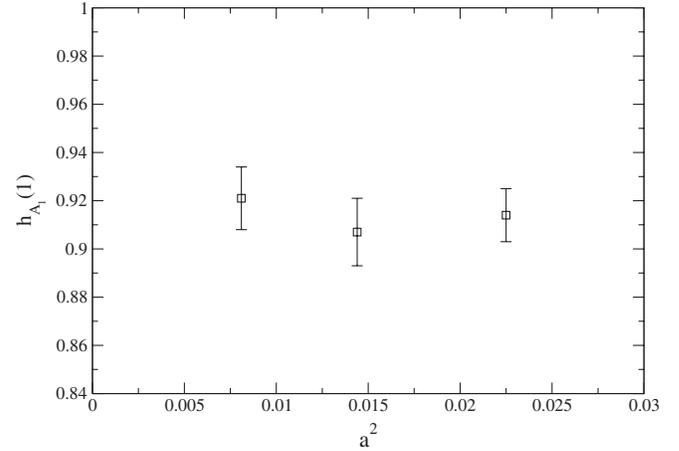| a (fm)	$h_{A_1}(1)$
0.15	0.914(11)
0.12	0.907(14)
0.09	0.921(13)

FIG. 9. $h_{A_1}(1)$ at physical quark masses versus a^2 (fm^2), where taste-violating effects have been removed, or shown to be negligible. Discretization effects due to analytic terms associated with the light-quark sector and heavy-quark discretization effects remain in the lattice data.

discretization errors coming from the light-quark analytic term and the heavy-quark discretization effects. Table IX presents the results for $h_{A_1}(1)$ as obtained from Eq. (43), and Fig. 9 shows them plotted as a function of lattice spacing squared. Although the Fermilab action and currents possess a smooth continuum limit, the MILC ensembles are not yet at small enough a to obtain simply $O(a)$ or $O(a^2)$ behavior. The spread of the lattice data points gives some indication of the size of the remaining discretization effects, however, and we find that the fine (0.09 fm) lattice data point and the coarse (0.12 fm) lattice data point differ by 1.5%. This is similar to our power-counting estimate, and we assign the larger of the two, 1.5%, as the systematic error due to residual discretization effects.

G. Summary

Our final result, given the error budget in Table X, is

$$h_{A_1} = 0.921(13)(8)(8)(14)(6)(3)(4), \qquad (45)$$

TABLE X. Final error budget for $h_{A_1}(1)$ where each error is discussed in the text. Systematic errors are added in quadrature and combined in quadrature with the statistical error to obtain the total error.

Uncertainty	$h_{A_1}(1)$
Statistics	1.4%
$g_{DD^*\pi}$	0.9%
NLO vs NNLO χPT fits	0.9%
Discretization errors	1.5%
Kappa tuning	0.7%
Perturbation theory	0.3%
u_0 tuning	0.4%
Total	2.6%

where the errors are statistical, parametric uncertainty in $g_{DD^*\pi}$, chiral extrapolation errors, discretization errors, parametric uncertainty in heavy-quark masses (kappa tuning), perturbative matching, and the u_0 (mis)tuning on the coarse lattices. Adding all systematic errors in quadrature, we obtain

$$h_{A_1}(1) = 0.921(13)(20). \qquad (46)$$

This final result differs slightly from that presented at Lattice 2007 [80], where a preliminary $h_{A_1}(1) = 0.924(12)(19)$ was quoted. There are three main changes in the analysis from the preliminary result: our earlier result used a value of α_s in the perturbative matching evaluated at the scale $2/a$, while the present result uses the HLM [64] prescription to fix the scale. This causes a change of 0.1%, well within the estimated systematic error due to the perturbative matching. In the previous result, the fine lattice data was blocked by 4 in the jackknife procedure; we now block by 8 to fully account for autocorrelation errors. This does not change the central value, but increases the statistical error slightly. Finally, we have chosen a value for $g_{DD^*\pi} = 0.51 \pm 0.2$ instead of $g_{DD^*\pi} = 0.45 \pm 0.15$ to be more consistent with the range of values quoted in the literature. This causes a decrease in $h_{A_1}(1)$ of 0.2%.

VIII. CONCLUSIONS

We have introduced a new method to calculate the zero-recoil form factor for the $B \to D^* \ell \nu$ decay. We include $2 + 1$ flavors of sea quarks in the generation of the gauge ensembles, so the calculation is completely unquenched. We have introduced a new double ratio, which gives the form factor directly, and leads to a large savings in the computational cost. The simulation is performed in a regime where we expect rooted staggered chiral perturbation theory to apply; we therefore use the rSχPT result for the $B \to D^*$ form factor [22] to perform the chiral extrapolation and to remove taste-breaking effects. To aid the chiral and continuum extrapolations, we introduced a set of ratios that has allowed us to largely disentangle light and heavy-quark discretization effects. Our new result $\mathcal{F}(1) = h_{A_1}(1) = 0.921(13)(20)$ is consistent with the previous quenched result $\mathcal{F}(1) = 0.913^{+0.029}_{-0.034}$ [13], but our errors are both smaller and under better theoretical control. This result allows us to extract $|V_{cb}|$ from the experimental measurement of the $B \to D^* \ell \nu$ form factor, which determines $\mathcal{F}(1)|V_{cb}|$. After applying a 0.7% electromagnetic correction to our value for $\mathcal{F}(1)$ [81], and taking the most recent PDG average for $|V_{cb}|\mathcal{F}(1) = (35.9 \pm 0.8) \times 10^{-3}$ [82], we find

$$|V_{cb}| = (38.7 \pm 0.9_{\text{exp}} \pm 1.0_{\text{theo}}) \times 10^{-3}. \qquad (47)$$

This differs by about 2σ from the inclusive determination $|V_{cb}| = (41.6 \pm 0.6) \times 10^{-3}$ [82]. Our new value supersedes the previous Fermilab quenched number [13], as it should other quenched numbers such as that in Ref. [83].[3]

Our largest error in $\mathcal{F}(1)$ is the systematic error due to heavy-quark discretization effects, which we have estimated using HQET power counting and inspection of the numerical data at three lattice spacings. This error can be reduced by going to finer lattice spacings, or by using an improved Fermilab action [70]. When using this improved action, it would be necessary to improve the currents to the same order. We have introduced a method for separating the heavy and light-quark discretization errors, where the physical h_{A_1} can be factorized into two factors $h_{A_1}^{\text{fid}} \times \mathcal{R}_{\text{fid}}$, such that the heavy-quark discretization errors are largely isolated in $h_{A_1}^{\text{fid}}$. Combining our value of $\mathcal{R}_{\text{fid}} = 0.997(10)(13)$ (where the first error is statistical, and the second is due to systematics that do not cancel in the ratio) with a determination of $h_{A_1}^{\text{fid}}$ at finer lattice spacings and/or with an improved action would be a cost-effective way of reducing the heavy-quark discretization errors. The next largest error in our calculation of $\mathcal{F}(1)$ is statistical, and this error drives many of the systematic errors. This is mostly a matter of computing. It would also be desirable to perform the matching of the heavy-quark current to higher order in perturbation theory, or by using nonperturbative matching. With these improvements, it would be possible to bring the error in $\mathcal{F}(1)$ to or below 1%, allowing a very precise determination of $|V_{cb}|$ from exclusive semileptonic decays.

---

[3]Ref. [83] calculates the $B \to D^* \ell \nu$ form factor in the quenched approximation at zero and nonzero recoil momentum and uses a step-scaling method [84] to control the heavy-quark discretization errors.

APPENDIX: CHIRAL PERTURBATION THEORY

Eq. (34) of Ref. [22] gives the expression needed for $h_{A_1}(1)$ in partially quenched χPT with degenerate up- and down-quark masses (the $2 + 1$ case) in the rooted staggered theory:

$$
\begin{aligned}
h_{A_1}^{(B_x)PQ,2+1}(1)/\eta_A = 1 + X_A(\Lambda_\chi) + \frac{g_{DD^*\pi}^2}{48\pi^2 f^2}\Bigg\{ &\frac{1}{16} \sum_{\substack{j=xu,xu,xs \\ \Xi=I,P,4V,4A,6T}} \bar{F}_{j\Xi} + \frac{1}{3}\Bigg[R_{X_I}^{[2,2]}(\{M_{X_I}^{(5)}\};\{\mu_I\})\Bigg(\frac{d\bar{F}_{X_I}}{dm_{X_I}^2}\Bigg) \\
&- \sum_{j\in\{M_I^{(5)}\}} D_{j,X_I}^{[2,2]}(\{M_{X_I}^{(5)}\};\{\mu_I\})\bar{F}_j \Bigg] + a^2\delta_V'\Bigg[R_{X_I}^{[3,2]}(\{M_{X_V}^{(7)}\};\{\mu_V\})\Bigg(\frac{d\bar{F}_{X_V}}{dm_{X_V}^2}\Bigg) - \sum_{j\in\{M_V^{(7)}\}} D_{j,X_V}^{[3,2]}(\{M_{X_V}^{(7)}\};\{\mu_V\})\bar{F}_j \Bigg] \\
&+ (V\to A)\Bigg\},
\end{aligned}
\tag{A1}
$$

where

$$
\begin{aligned}
F(m_j, z_j) &= \frac{m_j^2}{z_j}\Bigg\{ z_j^3 \ln\frac{m_j^2}{\Lambda_\chi^2} + \frac{1}{3}z_j^3 - 4z_j + 2\pi - \sqrt{z_j^2 - 1}(z_j^2 + 2)(\ln[1 - 2z_j(z_j - \sqrt{z_j^2 - 1})] - i\pi)\Bigg\} \\
&\to (\Delta^{(c)})^2 \ln\Bigg(\frac{m_j^2}{\Lambda_\chi^2}\Bigg) + \mathcal{O}[(\Delta^{(c)})^3],
\end{aligned}
\tag{A2}
$$

with $\bar{F}(m_j, z_j) = F(m_j, -z_j)$, and $z_j = \Delta^{(c)}/m_j$, where $\Delta^{(c)}$ is the D-D^* mass splitting. The residues $R_j^{[n,k]}$ and $D_{j,i}^{[n,k]}$ are defined in Refs. [18,19], and for completeness we quote them here:

$$
R_j^{[n,k]}(\{M\},\{\mu\}) \equiv \frac{\prod_{a=1}^k(\mu_a^2 - m_j^2)}{\prod_{i\neq j}(m_i^2 - m_j^2)}, \qquad D_{j,l}^{[n,k]}(\{M\},\{\mu\}) \equiv -\frac{d}{dm_l^2}R_j^{[n,k]}(\{M\},\{\mu\}).
\tag{A3}
$$

These residues are a function of two sets of masses, the numerator masses, $\{M\} = \{m_1, m_2, \ldots, m_n\}$ and the denominator masses, $\{\mu\} = \{\mu_1, \mu_2, \ldots, \mu_k\}$. In our $2 + 1$ flavor case, we have

$$
\{M_X^{(5)}\} \equiv \{m_\eta, m_X\}, \qquad \{M_X^{(7)}\} \equiv \{m_\eta, m_{\eta'}, m_X\}, \qquad \{\mu\} \equiv \{m_U, m_S\}.
\tag{A4}
$$

The masses $m_{\eta_I}, m_{\eta_V}, m_{\eta_V'}$ are given by [18]

$$
m_{\eta_I}^2 = \frac{m_{U_I}^2}{3} + \frac{2m_{S_I}^2}{3}, \qquad m_{\eta_V}^2 = \frac{1}{2}\Bigg(m_{U_V}^2 + m_{S_V}^2 + \frac{3}{4}a^2\delta_V' - Z\Bigg), \qquad m_{\eta_V'}^2 = \frac{1}{2}\Bigg(m_{U_V}^2 + m_{S_V}^2 + \frac{3}{4}a^2\delta_V' + Z\Bigg),
$$

$$
Z \equiv \sqrt{(m_{S_V}^2 - m_{U_V}^2)^2 - \frac{a^2\delta_V'}{2}(m_{S_V}^2 - m_{U_V}^2) + \frac{9(a^2\delta_V')^2}{16}}.
\tag{A5}
$$

The ratio $R_{\text{val}}^{\text{NLO}}$ in the continuum through NLO in χPT is

$$
\begin{aligned}
\mathcal{R}_{\text{val}}^{\text{NLO}} = 1 + \frac{g_{DD^*\pi}^2}{48\pi^2 f^2}\Bigg\{ &\sum_{j=u,d,s}\bar{F}_{xj} + \frac{1}{3}\Bigg[R_X^{[2,2]}(\{M_X^{(5)}\};\{\mu\})\Bigg(\frac{d\bar{F}_X}{dm_X^2}\Bigg) - \sum_{j\in\{M_X^{(5)}\}} D_{j,X}^{[2,2]}(\{M_X^{(5)}\};\{\mu\})\bar{F}_j \Bigg] \\
&- \sum_{j=u,d,s}\bar{F}_{x'j} - \frac{1}{3}\Bigg[R_{X'}^{[2,2]}(\{M_{X'}^{(5)}\};\{\mu\})\Bigg(\frac{d\bar{F}_{X'}}{dm_{X'}^2}\Bigg) - \sum_{j\in\{M_{X'}^{(5)}\}} D_{j,X'}^{[2,2]}(\{M_{X'}^{(5)}\};\{\mu\})\bar{F}_j \Bigg]\Bigg\},
\end{aligned}
\tag{A6}
$$

where

$$
\{M_{X'}^{(5)}\} \equiv \{m_\eta, m_{X'}\},
\tag{A7}
$$

and where $m_{X'}$ is a valence pion made of two quarks set to the fiducial valence quark mass, and the subscript x' refers to a valence quark at the fiducial mass. This ratio is one by construction when the valence quark mass equals the fiducial valence quark mass.

[1] E. Barberio *et al.* (Heavy Flavor Averaging Group (HFAG)), arXiv:0704.3575.

[2] E. Gamiz *et al.* (HPQCD Collaboration), Phys. Rev. D **73**, 114502 (2006).

[3] T. Bae, J. Kim, and W. Lee, Proc. Sci., LAT2005 (2006) 335 [arXiv:hep-lat/0510008].

[4] D. J. Antonio *et al.* (RBC Collaboration), Phys. Rev. Lett. **100**, 032001 (2008).

[5] C. Aubin, J. Laiho, and R. S. Van de Water, Proc. Sci., LAT2007 (2007) 375 [arXiv:0710.1121].

[6] J. Chay, H. Georgi, and B. Grinstein, Phys. Lett. B **247**, 399 (1990).

[7] I. I. Y. Bigi, N. G. Uraltsev, and A. I. Vainshtein, Phys. Lett. B **293**, 430 (1992).

[8] I. I. Y. Bigi, B. Blok, M. A. Shifman, N. G. Uraltsev, and A. I. Vainshtein, arXiv:hep-ph/9212227.

[9] I. I. Y. Bigi, M. A. Shifman, N. G. Uraltsev, and A. I. Vainshtein, Phys. Rev. Lett. **71**, 496 (1993).

[10] I. I. Y. Bigi, M. A. Shifman, and N. Uraltsev, Annu. Rev. Nucl. Part. Sci. **47**, 591 (1997).

[11] O. Büchmuller and H. Flächer, Phys. Rev. D **73**, 073008 (2006).

[12] C. W. Bauer, Z. Ligeti, M. Luke, A. V. Manohar, and M. Trott, Phys. Rev. D **70**, 094017 (2004).

[13] S. Hashimoto, A. S. Kronfeld, P. B. Mackenzie, S. M. Ryan, and J. N. Simone, Phys. Rev. D **66**, 014503 (2002).

[14] C. W. Bernard *et al.*, Phys. Rev. D **64**, 054506 (2001).

[15] C. Aubin *et al.*, Phys. Rev. D **70**, 094505 (2004).

[16] C. Aubin *et al.* (MILC Collaboration), Phys. Rev. D **70**, 114501 (2004).

[17] W.-J. Lee and S. R. Sharpe, Phys. Rev. D **60**, 114503 (1999).

[18] C. Aubin and C. Bernard, Phys. Rev. D **68**, 034014 (2003).

[19] C. Aubin and C. Bernard, Phys. Rev. D **68**, 074011 (2003).

[20] S. R. Sharpe and R. S. Van de Water, Phys. Rev. D **71**, 114505 (2005).

[21] C. Aubin and C. Bernard, Nucl. Phys. B, Proc. Suppl. **140**, 491 (2005).

[22] J. Laiho and R. S. Van de Water, Phys. Rev. D**73**, 054501 (2006).

[23] A. F. Falk and M. Neubert, Phys. Rev. D **47**, 2965 (1993).

[24] T. Mannel, Phys. Rev. D **50**, 428 (1994).

[25] A. Czarnecki, Phys. Rev. Lett. **76**, 4124 (1996).

[26] A. Czarnecki and K. Melnikov, Nucl. Phys. **B505**, 65 (1997).

[27] M. E. Luke, Phys. Lett. B **252**, 447 (1990).

[28] A. S. Kronfeld, Phys. Rev. D **62**, 014505 (2000).

[29] J. Harada *et al.*, Phys. Rev. D **65**, 094513 (2002).

[30] J. Harada, S. Hashimoto, A. S. Kronfeld, and T. Onogi, Phys. Rev. D **65**, 094514 (2002).

[31] S. Prelovsek, Phys. Rev. D **73**, 014506 (2006).

[32] C. W. Bernard, C. E. DeTar, Z. Fu, and S. Prelovsek, Proc. Sci., LAT2006 (2006) 173.

[33] C. Bernard, Phys. Rev. D **73**, 114503 (2006).

[34] C. Bernard, C. E. Detar, Z. Fu, and S. Prelovsek, Phys. Rev. D **76**, 094504 (2007).

[35] C. Aubin, J. Laiho, and R. S. Van de Water, Phys. Rev. D **77**, 114501 (2008).

[36] C. Bernard, M. Golterman, and Y. Shamir, Phys. Rev. D **73**, 114511 (2006).

[37] Y. Shamir, Phys. Rev. D **75**, 054503 (2007).

[38] Y. Shamir, Phys. Rev. D **71**, 034509 (2005).

[39] S. Dürr, Proc. Sci., LAT2005 (2005) 021 [arXiv:hep-lat/0509026].

[40] S. R. Sharpe, Proc. Sci., LAT2006 (2006) 022 [arXiv:hep-lat/0610094].

[41] A. S. Kronfeld, Proc. Sci., LAT2007 (2007) 016 [arXiv:0711.0699].

[42] T. Blum *et al.*, Phys. Rev. D **55**, R1133 (1997).

[43] K. Orginos and D. Toussaint (MILC Collaboration), Phys. Rev. D **59**, 014501 (1998).

[44] J. F. Lagae and D. K. Sinclair, Phys. Rev. D **59**, 014511 (1998).

[45] G. P. Lepage, Phys. Rev. D **59**, 074502 (1999).

[46] K. Orginos, D. Toussaint, and R. L. Sugar (MILC Collaboration), Phys. Rev. D **60**, 054503 (1999).

[47] C. W. Bernard *et al.* (MILC Collaboration), Phys. Rev. D **61**, 111502 (2000).

[48] B. Sheikholeslami and R. Wohlert, Nucl. Phys. **B259**, 572 (1985).

[49] A. X. El-Khadra, A. S. Kronfeld, and P. B. Mackenzie, Phys. Rev. D **55**, 3933 (1997).

[50] G. P. Lepage and P. B. Mackenzie, Phys. Rev. D **48**, 2250 (1993).

[51] R. Sommer, Nucl. Phys. **B411**, 839 (1994).

[52] C. W. Bernard *et al.* (MILC Collaboration), Phys. Rev. D **62**, 034503 (2000).

[53] A. Gray *et al.* (HPQCD Collaboration), Phys. Rev. Lett. **95**, 212001 (2005).

[54] C. Bernard (MILC Collaboration), Proc. Sci., LAT2007 (2007) 090 [arXiv:0710.1118].

[55] C. Bernard *et al.* (MILC Collaboration), Proc. Sci., LAT2005 (2006) 025 [arXiv:hep-lat/0509137].

[56] M. Wingate, J. Shigemitsu, C. T. Davies, G. P. Lepage, and H. D. Trottier, Phys. Rev. D **67**, 054505 (2003).

[57] M. Okamoto *et al.*, Nucl. Phys. B, Proc. Suppl. **140**, 461 (2005).

[58] C. Aubin *et al.* (Fermilab Lattice), Phys. Rev. Lett. **94**, 011601 (2005).

[59] C. Aubin *et al.*, Phys. Rev. Lett. **95**, 122002 (2005).

[60] E. Dalgic *et al.*, Phys. Rev. D **73**, 074502 (2006).

[61] R. T. Evans, A. X. El-Khadra, and M. Di Pierro (Fermilab Lattice and MILC Collaborations), Proc. Sci., LAT2006 (2006) 081.

[62] S. J. Brodsky, G. P. Lepage, and P. B. Mackenzie, Phys. Rev. D **28**, 228 (1983).

[63] Q. Mason *et al.* (HPQCD Collaboration), Phys. Rev. Lett. **95**, 052002 (2005).

[64] K. Hornbostel, G. P. Lepage, and C. Morningstar, Phys. Rev. D **67**, 034023 (2003).

[65] A. X. El-Khadra, E. Gamiz, A. S. Kronfeld, and M. A. Nobes, Proc. Sci., LAT2007 (2007) 242 [arXiv:0710.1437].

[66] A. X. El-Khadra, E. Gamiz, A. S. Kronfeld, and M. A. Nobes (unpublished).

[67] G. P. Lepage, J. Comput. Phys. **27**, 192 (1978).

[68] C. Aubin and C. Bernard, Phys. Rev. D **73**, 014515 (2006).

[69] C. Bernard, M. Golterman, and Y. Shamir, Phys. Rev. D **77**, 074505 (2008).

[70] M. B. Oktay and A. S. Kronfeld, Phys. Rev. D **78**, 014504 (2008).

[71] E. Follana *et al.* (HPQCD Collaboration), Phys. Rev. D **75**, 054502 (2007).

[72] A. S. Kronfeld, Nucl. Phys. B, Proc. Suppl. **53**, 401 (1997).

[73] I. W. Stewart, Nucl. Phys. **B529**, 62 (1998).

[74] M. C. Arnesen, B. Grinstein, I. Z. Rothstein, and I. W. Stewart, Phys. Rev. Lett. **95**, 071802 (2005).

[75] R. Casalbuoni *et al.*, Phys. Rep. **281**, 145 (1997).

[76] A. Abada *et al.*, Nucl. Phys. B, Proc. Suppl. **119**, 641 (2003).

[77] H. Ohki, H. Matsufuru, and T. Onogi, Phys. Rev. D **77**, 094509 (2008).

[78] A. Anastassov *et al.* (CLEO Collaboration), Phys. Rev. D **65**, 032003 (2002).

[79] D. Arndt and C. J. D. Lin, Phys. Rev. D **70**, 014503 (2004).

[80] J. Laiho (Fermilab Lattice and MILC Collaborations), Proc. Sci., LAT2007 (2007) 358 [arXiv:0710.1111].

[81] A. Sirlin, Nucl. Phys. **B196**, 83 (1982).

[82] C. Amsler *et al.* (Particle Data Group), Phys. Lett. B **667**, 1 (2008).

[83] G. M. de Divitiis, R. Petronzio, and N. Tantalo, Nucl. Phys. **B807**, 373 (2009).

[84] M. Guagnelli, F. Palombi, R. Petronzio, and N. Tantalo, Phys. Lett. B **546**, 237 (2002).